

REVIEW

Tropical Temperature Variability in the UTLS: New Insights from GPS Radio Occultation Observations

BARBARA SCHERLLIN-PIRSCHER,^{a,b} ANDREA K. STEINER,^{b,c} RICHARD A. ANTHES,^d M. JOAN ALEXANDER,^e
SIMON P. ALEXANDER,^f RICCARDO BIONDI,^g THOMAS BIRNER,^h JOOWAN KIM,ⁱ WILLIAM J. RANDEL,^j
SEOK-WOO SON,^k TOSHITAKA TSUDA,^l AND ZHEN ZENG^d

^a *Zentralanstalt für Meteorologie und Geodynamik, Graz, Austria*

^b *Wegener Center for Climate and Global Change, University of Graz, Graz, Austria*

^c *Institute for Geophysics, Astrophysics, and Meteorology, Institute of Physics, University of Graz, Graz, Austria*

^d *COSMIC Program Office, University Corporation for Atmospheric Research, Boulder, Colorado*

^e *NorthWest Research Associates/Colorado Research Associates, Boulder, Colorado*

^f *Australian Antarctic Division, Hobart, Tasmania, Australia*

^g *Dipartimento di Geoscienze, Università degli Studi di Padova, Padua, Italy*

^h *Ludwig Maximilian University, Munich, Germany*

ⁱ *Department of Atmospheric Sciences, Kongju National University, Gongju, South Korea*

^j *Atmospheric Chemistry, Observations and Modeling Laboratory, National Center for Atmospheric Research, Boulder, Colorado*

^k *School of Earth and Environmental Sciences, Seoul National University, Seoul, South Korea*

^l *Research Institute for Sustainable Humanosphere, Kyoto University, Uji, Japan*

(Manuscript received 23 May 2020, in final form 24 September 2020)


ABSTRACT: Global positioning system (GPS) radio occultation (RO) observations, first made of Earth's atmosphere in 1995, have contributed in new ways to the understanding of the thermal structure and variability of the tropical upper troposphere–lower stratosphere (UTLS), an important component of the climate system. The UTLS plays an essential role in the global radiative balance, the exchange of water vapor, ozone, and other chemical constituents between the troposphere and stratosphere, and the transfer of energy from the troposphere to the stratosphere. With their high accuracy, precision, vertical resolution, and global coverage, RO observations are uniquely suited for studying the UTLS and a broad range of equatorial waves, including gravity waves, Kelvin waves, Rossby and mixed Rossby–gravity waves, and thermal tides. Because RO measurements are nearly unaffected by clouds, they also resolve the upper-level thermal structure of deep convection and tropical cyclones as well as volcanic clouds. Their low biases and stability from mission to mission make RO observations powerful tools for studying climate variability and trends, including the annual cycle and intraseasonal-to-interannual atmospheric modes of variability such as the quasi-biennial oscillation (QBO), Madden–Julian oscillation (MJO), and El Niño–Southern Oscillation (ENSO). These properties also make them useful for evaluating climate models and detection of small trends in the UTLS temperature, key indicators of climate change. This paper reviews the contributions of RO observations to the understanding of the three-dimensional structure of tropical UTLS phenomena and their variability over time scales ranging from hours to decades and longer.

KEYWORDS: Tropics; Stratosphere-troposphere coupling; Upper troposphere; Temperature; Occultation; Tropical variability

1. Introduction

The thermal structure and variability of the tropical upper troposphere–lower stratosphere (UTLS) are fundamental to many aspects of the climate system. Tropical temperatures decrease with height from the surface to the tropopause near 17 km (Fig. 1) and then increase with height in the stratosphere. The UTLS region refers to the broad altitude layer over ~12–22 km, spanning the transition from the relatively well-mixed

convective troposphere to the stably stratified lower stratosphere. The chemical composition also changes sharply across this layer, including species such as ozone, carbon monoxide, and water vapor. A somewhat narrower layer centered around the tropical tropopause, that is, ~14–19 km, is also referred to as the tropical tropopause layer (TTL; e.g., Fueglistaler et al. 2009; Randel and Jensen 2013). Temperatures in the UTLS are strongly coupled to large- and small-scale circulations and deep convection (with likely two-way coupling) and are important for controlling UTLS cirrus and aerosol behavior and, hence, radiative balances. Further, temperatures at the tropical

 Denotes content that is immediately available upon publication as open access.

Corresponding author: Barbara Scherllin-Pirscher, barbara.scherllin-pirscher@zamg.ac.at

DOI: 10.1175/JCLI-D-20-0385.1



This article is licensed under a [Creative Commons Attribution 4.0 license](http://creativecommons.org/licenses/by/4.0/) (<http://creativecommons.org/licenses/by/4.0/>).

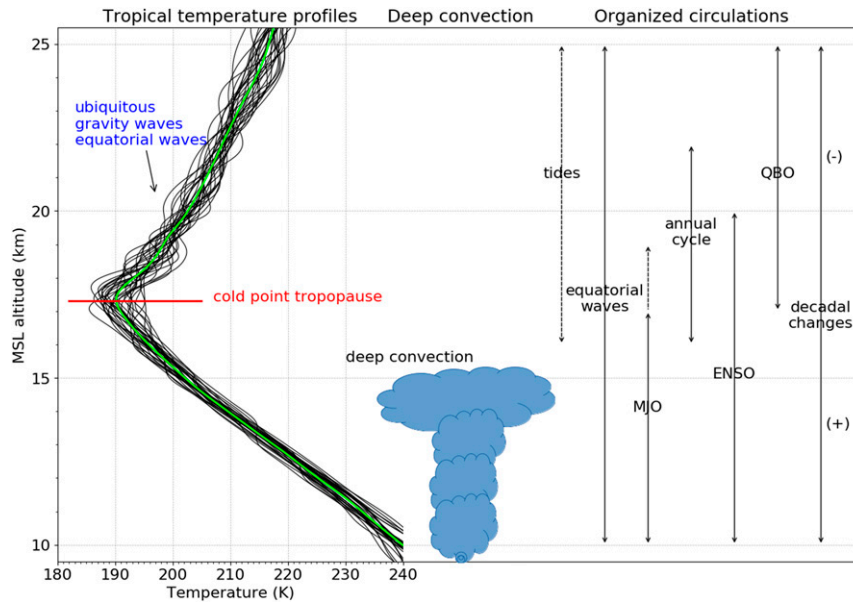


FIG. 1. (left) Example tropical temperature profiles obtained from RO measurements (black) and their mean profile (green), (center) approximate vertical scale of tropical deep convective clouds, and (right) the vertical extent of various large-scale organized temperature signals in the tropical UTLS, many of them related directly or indirectly to tropical deep convection.

tropopause exert a strong control on global stratospheric water vapor via dehydration of air entering the stratosphere across the cold tropopause (Brewer 1949; Mote et al. 1996; Randel and Park 2019).

Tropical UTLS temperatures are characterized by large variability in space and time, especially near the tropopause, as illustrated by the example profiles in Fig. 1. Much of the variability occurs with relatively small vertical scales, associated with a broad spectrum of large- and small-scale waves and various atmospheric circulations with a range of diurnal-to-interannual time scales (Fig. 1) (e.g., Salby and Garcia 1987; Alexander 1996). This thermal variability is clearly observed in high-resolution radiosonde observations (Tsuda et al. 1994; Kim and Alexander 2015) but is less well resolved in nadir-sounding satellite measurements or meteorological analyses/reanalyses with typical vertical resolution of 1 km or greater. In contrast, Global Navigation Satellite System (GNSS) radio occultation (RO) measurements provide high-vertical-resolution (of order 100 m) soundings and thus sensitivity to short-vertical-scale UTLS features (Noersomadi and Tsuda 2017; Zeng et al. 2019). The dense sampling and two-decade-long RO record provide novel information on UTLS thermal behaviors and their links to processes spanning the wide range of scales indicated in Fig. 1. RO observations, with their small biases, also serve as “anchor” observations in forecast models and reanalyses and are assimilated in several reanalyses without bias corrections, unlike satellite radiance measurements (Fujiwara et al. 2017). This review is intended to summarize this information and demonstrate the added value of RO data

with regard to the tropical UTLS in combination with other measurements and analyzed meteorological products.

2. Radio occultation data

a. Occultation geometry and retrieval

RO is an active remote sensing technique that exploits electromagnetic signals transmitted by a GNSS satellite at two (or more) L-band microwave frequencies with wavelengths of about 20 cm. GNSS includes GPS, Globalnaya Navigatsionnaya Sputnikovaya Sistema (GLONASS), and other systems, but so far mainly GPS signals have been used for RO measurements. These signals travel through the atmosphere, where they are refracted due to ionospheric and neutral atmospheric vertical density gradients (e.g., Melbourne et al. 1994; Syndergaard 1999; Yunck et al. 2000). A receiver on a satellite in low-Earth orbit (LEO) records the signals in an oblique vertical scan of the atmosphere due to the relative motion of the two satellites (Foelsche et al. 2011a). RO geometry is shown in Fig. 2.

Basic observables are the GNSS signals' excess phases (excess compared to propagation in vacuum), which can be converted to bending angle profiles. Linearly combining the bending angles that are derived from the two L-band frequencies (L1 and L2 bending angles) removes most of the ionospheric contribution to the measurement. Atmospheric refractivity is obtained from the neutral atmospheric bending angle. This step requires accurate information about the atmospheric state at high altitudes (e.g., above 55 km; Ao et al.

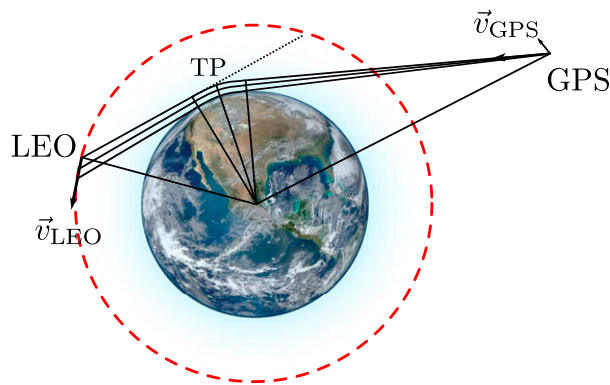


FIG. 2. Geometry of a setting RO event. The RO measurement profile is obtained along the tangent point (TP) trajectory.

2006), which is usually not available from RO measurements as noise overshadows the weak RO signal at high altitudes. Therefore, some a priori information about the atmospheric state at high altitudes is used in this step. Refractivity in the neutral atmosphere depends mainly on temperature, pressure, and water vapor pressure. In the UTLS region, however, the amount of water vapor is negligibly small. There, temperature can be computed directly from refractivity (Kursinski et al. 1997; Leroy 1997; Scherllin-Pirscher et al. 2017b). In the moist atmosphere, temperature and humidity are retrieved with additional background information (Ware et al. 1996; Rieckh et al. 2018; Li et al. 2019). Details about the retrieval process are given by Melbourne et al. (1994), Kursinski et al. (1997), Syndergaard (1999), Hajj et al. (2002), and Steiner et al. (2011).

Mean fields of atmospheric parameters are obtained by gridding and averaging (e.g., Foelsche et al. 2008a) or statistical Bayesian interpolation (Leroy et al. 2012) of individual profiles. Alternatively, mean profiles of bending angle are propagated through the retrieval (Ao et al. 2012; Gleisner and Healy 2013; Danzer et al. 2014b, 2018). Climatological geopotential fields can then be used to derive averaged wind fields outside the tropics using geostrophic or gradient wind approximations (Scherllin-Pirscher et al. 2014; Verkhoglyadova et al. 2014; Healy et al. 2020).

b. Data characteristics

Advantages of RO measurements are manifold. Data characteristics are summarized in Table 1. The occultation geometry (Fig. 2) yields high-vertical-resolution profiles (e.g., Noersomadi and Tsuda 2017) with an effective vertical resolution ranging from 0.1 km near the tropical tropopause to about 1.4 km in the polar lower stratosphere (Zeng et al. 2019). A caveat is that the horizontal averaging inherent in RO (over ~ 200 km) and altitude variations along the ray path can combine to limit the effective vertical resolution to ~ 1 km, which is important for atmospheric wave analyses. Due to the use of microwave signals, measurements can be performed during day and night and penetrate through clouds. Since RO measurements are based on precise atomic clocks, they are traceable to the International System of Units (Leroy et al. 2006b). Exploitation of relative rather than absolute phase measurements additionally ensures

self-calibration, long-term stability, and high precision of measurement profiles. Measurements are therefore independent of the satellite and data from different satellites can be combined to create consistent long-term RO records. In the UTLS region, long-term stability and high precision are also valid for derived atmospheric RO variables as shown by Hajj et al. (2004), Schreiner et al. (2007), Foelsche et al. (2011b), Steiner et al. (2011), Angerer et al. (2017), and Steiner et al. (2020a).

Uncertainty (random errors) of individual RO profiles is smallest in the UTLS region, where it amounts to approximately 0.7 K for dry temperature (Scherllin-Pirscher et al. 2011b). Comparisons to other measurements, analyses, and reanalyses have demonstrated the high accuracy (low biases) of RO atmospheric profiles in the UTLS (e.g., Schröder et al. 2003; Wang et al. 2004; Kuo et al. 2005; Gobiet et al. 2007; Ho et al. 2007; Steiner et al. 2007; Foelsche et al. 2008a). In most cases, a large part of the difference was attributed to biases of the comparison datasets, such as the varying quality of different radiosonde types (e.g., He et al. 2009; B.-R. Wang et al. 2013), biases in daytime radiosonde measurements (Sun et al. 2010; Ladstädter et al. 2015; Tradowsky et al. 2017) or changes in analysis or reanalysis systems (Angerer et al. 2017; Shangguan et al. 2019; Ho et al. 2020). Important for all these comparison studies is to appropriately minimize representativeness and sampling errors of all correlative datasets (e.g., Ladstädter et al. 2011; Feltz et al. 2014; Gilpin et al. 2018). On a long-term basis, residual biases from ionospheric contributions to the RO measurement, which depend on solar activity, cannot be neglected as they can be as high as 2 K at 30 km during high solar activity (Danzer et al. 2013). Application of an ionospheric error model (Healy and Culverwell 2015), however, can significantly reduce this error (Danzer et al. 2015).

For climate applications, consistent long-term data records are required. RO measurements are stable over time and intersatellite biases are small (< 0.1 K between 8 and 25 km; Angerer et al. 2017). However, background information from the high altitude initialization enters the retrieval at the refractivity level and background biases can propagate down into the stratosphere and affect processing results. Early RO intercomparison studies of Ao et al. (2003), von Engeln (2006), Staten and Reichler (2008), and Löscher et al. (2009) found considerable differences among RO products from different processing centers. Close cooperation among major RO processing centers started in 2007 to systematically investigate these differences and to improve data processing. Studies of Ho et al. (2009, 2012) and Steiner et al. (2013, 2020a) significantly increased knowledge and understanding of these differences and revealed larger differences above approximately 25 km resulting from varying high-altitude initialization methods. Even though differences between processing centers have decreased over time, merging data from different processing schemes for climate applications is not recommended, but rather one should use data from an ensemble of RO records.

c. RO missions and processing centers

The first RO measurements of Earth's atmosphere were obtained by the proof-of-concept mission GPS/Meteorology

TABLE 1. Characteristics of the measurements and dry temperature profiles in the UTLS.

Property	Key references
<i>Number and distribution of RO measurements</i>	Jim et al. (2011) , Angerer et al. (2017) , and Schreiner et al. (2020)
2001–06: ~200 globally distributed profiles per day	
2006: Increase to more than 2000 globally distributed profiles per day	
2006–19: Global number of profiles per day varies between 1000 and 3000	
2019 onward: 7000 profiles per day, mainly between 45°S and 45°N	
<i>Clouds</i>	Kursinski et al. (1997) and Scherllin-Pirscher et al. (2011a)
Measurements are available in cloudy regions because GNSS signals can penetrate through clouds	
Limitation: In humid regions, RO dry temperature deviates from (real) physical temperature; differences increase with increasing humidity	
<i>Vertical range</i>	Kursinski et al. (1997) , Foelsche et al. (2008a) , and Zeng et al. (2019)
RO neutral atmospheric measurements are performed from the lowest troposphere to ~80 km (and above)	
RO core region of retrieved dry temperature profiles: ~8–30 km	
<i>Vertical resolution</i>	Kursinski et al. (1997) , Noersomadi and Tsuda (2017) , and Zeng et al. (2019)
~0.1 km near the tropical tropopause	
~1.5 km in the polar lower stratosphere	
<i>Horizontal averaging scale (or observation footprint or horizontal resolution)</i>	Melbourne et al. (1994) , Kursinski et al. (1997) , and Anthes et al. (2000)
About 1.5 km cross track	
About 250 km along the ray path	
<i>SI traceability</i>	Leroy et al. (2006b) , Ho et al. (2009) , and Schreiner et al. (2011)
RO measurements are based on accurate atomic clocks and therefore are traceable to the SI second	
Limitation: Current derived products are not SI traceable	
<i>Self-calibration and long-term stability</i>	Kursinski et al. (1997) , Danzer et al. (2014a) , and Angerer et al. (2017)
The measurement and the early retrieval stages are based on phase changes rather than on absolute phases; therefore, the measurements are stable over the long term and no data calibration is needed; data from different satellites can be combined to a single record	
Limitations: (i) Long-term stability of retrieved data is degraded by the use of background information in the retrieval process; (ii) variations of solar activity, which can leave a nonnegligible ionospheric residual; and (iii) the amount of humidity, which affects RO dry atmosphere parameters	
→ Data stability is highest from 8 to 30 km	
<i>Precision (uncertainty)</i>	Kuo et al. (2004) , Hajj et al. (2004) , Steiner and Kirchengast (2005) , Schreiner et al. (2007) , Scherllin-Pirscher et al. (2011a,b, 2017b) , Schwarz et al. (2017) , Sjoberg et al. (2021) , and Schreiner et al. (2020)
Random error variance or standard deviation	
Significantly decreases with a large number of profiles for mean atmospheric fields	
→ Highest precision/smallest uncertainty (~0.7 K for individual profiles) in the UTLS	
<i>Accuracy (biases/systematic errors)</i>	He et al. (2009) , Sun et al. (2010) , Feltz et al. (2014) , Ladstädter et al. (2015) , Ho et al. (2020) , and Tegtmeier et al. (2020)
Comparisons with radiosondes, microwave and infrared sounders, model analyses, and reanalyses	
→ Most comparisons revealed deficiencies in the comparison datasets	
→ Highest accuracy (smallest biases/systematic errors) of RO data in the UTLS; typical estimates are ~0.1 K from 8 to 30 km	

TABLE 1. (Continued)

Property	Key references
<p><i>Sampling error (difference between a sample value and a population mean in space and/or time; arises from atmospheric variability and limited spatiotemporal sampling)</i></p> <p>Typically <0.3 K in the tropical UTLS; if the sampling error is estimated and subtracted, the residual sampling error is ~30% of the original sampling error</p>	Pirscher et al. (2007), Foelsche et al. (2008a), and Scherllin-Pirscher et al. (2011b)
<p><i>Structural uncertainty (uncertainty arising from different choices in processing of the same raw data)</i></p> <p>Smallest structural uncertainty in the UTLS; <0.1 K from 8 to 30 km</p>	Ho et al. (2009, 2012) and Steiner et al. (2013, 2020a)

(GPS/MET) in 1995 (Ware et al. 1996; Hocke 1997; Rocken et al. 1997; Feng and Herman 1999). After GPS/MET successfully demonstrated the capability of RO, a number of RO satellite missions were launched in the following decade, significantly increasing the available number of measurements. Single satellites *Satellite de Aplicaciones Científico-C (SAC-C; Hajj et al. 2004)* and *Challenging Minisatellite Payload (CHAMP; Wickert et al. 2001a,b, 2003, 2004)* as well as the twin satellites of the Gravity Recovery and Climate Experiment (GRACE; the satellites are named *GRACE-A* and *GRACE-B* and are also referred to as *GRACE-1* and *GRACE-2*) (Wickert et al. 2005) provided the first multiyear RO satellite records. A big step forward to establish RO in the atmospheric scientific community was taken in 2006 with the launch of the Formosa Satellite Mission 3/Constellation Observing System for Meteorology, Ionosphere and Climate (FORMOSAT-3/COSMIC; Rocken et al. 2000; Anthes et al. 2008; Ho et al. 2020) constellation of six satellites and the first MetOp satellite (Luntama et al. 2008; von Engelmann et al. 2009).

COSMIC increased the global number of daily profiles from about 200 to more than 2000 (Jin et al. 2011; Angerer et al. 2017). Additional measurements from the *Terra Synthetic Aperture Radar at X Band (TerraSAR-X)*, *TerraSAR-X Add-On for Digital Elevation Measurement (TanDEM-X)*, and *Communications/Navigation Outage Forecast System (C/NIFS)* (see <https://earth.esa.int/web/eoportal/satellite-missions> for a summary of these missions) increased measurement density in the late 2000s. Recently launched *MetOp-C*, *Fengyun-3C* (Sun et al. 2018), and COSMIC-2 (Anthes and Schreiner 2019; Schreiner et al. 2020) ensure the continuity of the RO record to be used in atmospheric and climate sciences for the next five years at least.

Depending on the RO mission and retrieval product, RO data are made available by the Danish Meteorological Institute (DMI; <http://www.romsaf.org>), EUMETSAT (<http://www.eumetsat.int>), the German Research Centre for Geosciences (GFZ; <http://www.gfz-potsdam.de/en/section/space-geodetic-techniques/topics/gnss-radio-occultation/>), Jet Propulsion Laboratory (JPL; <https://genesis.jpl.nasa.gov/genesis/>), COSMIC Project Office, University Corporation for Atmospheric Research (UCAR; <http://cdaac-www.cosmic.ucar.edu>), and the Wegener Center for Climate and Global Change, University of Graz (WEGC; <http://www.wegcenter.at>). Information on the consistency and structural

uncertainty of multisatellite RO data from the different processing centers is given by Steiner et al. (2013, 2020a) including a detailed description of the RO retrieval and of the center-specific processing steps.

3. Tropopause structure

A detailed understanding of the processes that determine the temperature structure of the tropical tropopause is important for our understanding of stratospheric water vapor content and vertical wave propagation [with potential effects on the associated wave forcing of stratospheric winds, e.g., related to the quasi-biennial oscillation (QBO)]. The RO data are especially helpful in characterizing the tropical tropopause where high-vertical-resolution data (e.g., radiosondes) are sparse, meteorological analyses are not well constrained (Borsche et al. 2007; Tegtmeier et al. 2020), and climate models show large uncertainties (Gettelman et al. 2010; Kim et al. 2013).

a. Thermal tropopause

In the tropics the transition from the troposphere to the stratosphere does not take place across a single interface but rather across a layer, the so-called tropical tropopause layer (Fueglistaler et al. 2009). The TTL roughly extends from the top of main convective outflow near 150 hPa (~14 km in altitude) to the highest level of convective tops near 70 hPa (~18.5 km in altitude). Near the bottom of the TTL the temperature lapse rate starts to depart more strongly from a moist adiabat, whereas near the top of the TTL stratospheric temperature lapse rates are observed and static stability maximizes.

Although the concept of the TTL is physically more appropriate than a single tropopause interface, various tropopause definitions (i.e., thermal, dynamical, and chemical tropopauses) are still widely used in the literature. The thermal tropopauses, including the lapse-rate tropopause (LRT) and cold-point tropopause (CPT), are based on the temperature structure of the TTL and well defined across the tropics, with the CPT perhaps being the more physically relevant level because of its direct connection to the amount of water vapor that may enter the stratosphere. A dynamical tropopause based on a potential vorticity (PV) isosurface, however, is not applicable near the equator

where PV switches sign from negative values in the Southern Hemisphere to positive values in the Northern Hemisphere.

The LRT is conventionally defined as the lowest level at which the temperature lapse rate drops below 2 K km^{-1} , provided that its average between this level and all higher levels within 2 km remains below this threshold (WMO 1957). Multiple LRT levels have been diagnosed in the tropics (e.g., Schmidt et al. 2006; Randel et al. 2007) but are generally rare when compared with the subtropics and midlatitudes (e.g., Rieckh et al. 2014; Wilhelmsen et al. 2020).

In the case of RO data, a distinct tropopause level may also be identified based on the structure of the bending angle profile (Narayana Rao et al. 2007; Lewis 2009; Vespe et al. 2017), which has the advantage that it is based on raw data independent of uncertainties in the retrieval procedure.

Unlike throughout the free tropical troposphere, temperature near the tropical tropopause shows strong spatial and temporal variability (e.g., Randel et al. 2003; Scherllin-Pirscher et al. 2017a). This may be heuristically understood based on the long radiative time scales (~ 60 days) that are observed near the tropical tropopause: a seemingly unimportant heating rate of 0.1 K day^{-1} could result in a temperature perturbation of $\sim 6 \text{ K}$ over 60 days (cf. Birner and Charlesworth 2017). The RO data have been instrumental in quantifying these sources of variability from observations with quasi-homogenous coverage throughout the tropics. This was first demonstrated by GPS/MET (Nishida et al. 2000; Randel et al. 2003), extended to CHAMP (Schmidt et al. 2004, 2005), and later further extended to COSMIC (Son et al. 2011).

The CPT is simply the level corresponding to the minimum temperature in a given profile and is generally located somewhat higher than the LRT (e.g., Munchak and Pan 2014). The RO data reveal that CPT temperatures show a pronounced minimum over the western Pacific warm pool with values often dropping below 190 K, especially during boreal winter (Fig. 3). This minimum is consistent with the general tendency of a reduction in CPT temperature above regions of active deep convection [Randel et al. 2003; cf. low outgoing longwave radiation (OLR) values in Fig. 3]. Likewise, CPT temperatures are higher above regions of suppressed deep convection, such as above the eastern Pacific Ocean. In general, the distribution of CPT temperature reflects the large-scale quasi-stationary temperature response to convective heating (Matsuno 1966; Gill 1980, see also section 6). The RO data have also been used as a baseline for large-scale spatial variations as well as subseasonal, seasonal, and longer time-scale variations in CPT temperature and height.

Much of the temporal variability in CPT characteristics on subseasonal time scales is associated with wave perturbations, such as those that arise due to equatorial gravity and Kelvin waves (Randel et al. 2003). The Madden-Julian oscillation (MJO) also gives rise to variations in CPT characteristics (Zeng et al. 2012; Virts and Wallace 2014). Waves have been further shown to cause enhanced CPT temperature minima affecting cirrus formation (e.g., Mehta et al. 2011, 2013; Kim and Alexander 2015; J.-E. Kim et al. 2016; Son et al. 2017).

On interannual time scales the main drivers of CPT variability are El Niño–Southern oscillation (ENSO), QBO, and the occurrence of sudden stratospheric warmings (via

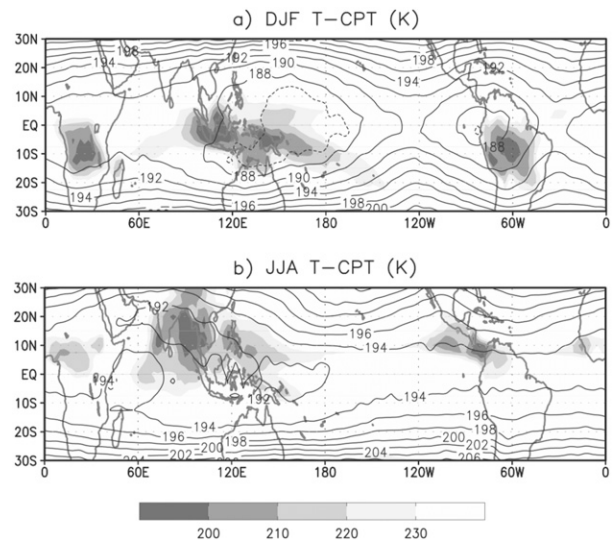


FIG. 3. Seasonal-mean CPT temperature in (a) December–February (DJF) and (b) June–August (JJA) based on COSMIC RO observations for the period from September 2006 to August 2010. Gray shading shows OLR (W m^{-2}) (Kim and Son 2012).

corresponding modulation of tropical upwelling within the Brewer–Dobson circulation), all of which have been quantified using RO data (Rieckh et al. 2014). Estimating decadal-scale tropopause variations from RO data is limited by its comparatively short record (about 20 years). Shorter-term trends have nevertheless been considered, such as for the CHAMP period from 2001 to 2007 (Schmidt et al. 2008b, 2010b; W. Wang et al. 2013).

b. Tropopause inversion layer

The tropopause inversion layer (TIL) is characterized by strongly increasing temperature with height and therefore strongly enhanced values of static stability just above the local tropopause. In the tropics, a broad layer of enhanced static stability exists between the tropopause and $\sim 23 \text{ km}$ altitude (Grise et al. 2010) that is fairly well resolved in reanalyses and models (Birner et al. 2006). However, a strong static stability maximum, which is confined to a thin layer just above the local tropopause ($\sim 1 \text{ km}$), can only be detected in high-vertical-resolution data such as RO and radiosondes (Bell and Geller 2008). Unlike radiosondes, which are sparsely distributed in the tropics, RO data allow a quantification of characteristics of such a thin TIL throughout the tropics (Grise et al. 2010; Schmidt et al. 2010a; Son et al. 2011). Figure 4 shows that the zonal-mean tropical TIL exists throughout the year, is strongest close to the equator, and shows strong seasonality at the edge of the tropics with enhanced values in the respective summer hemisphere. During boreal winter secondary stability maxima occur centered near 19 km over 10° – 20°N and 10° – 20°S , which are related to seasonally varying quasi-stationary tropical waves (e.g., Dima and Wallace 2007). On interannual time scales, Kumar et al. (2014) have shown that the tropical TIL is stronger during the westerly phase of the QBO. Pilch Kedzierski et al. (2016) have furthermore documented a

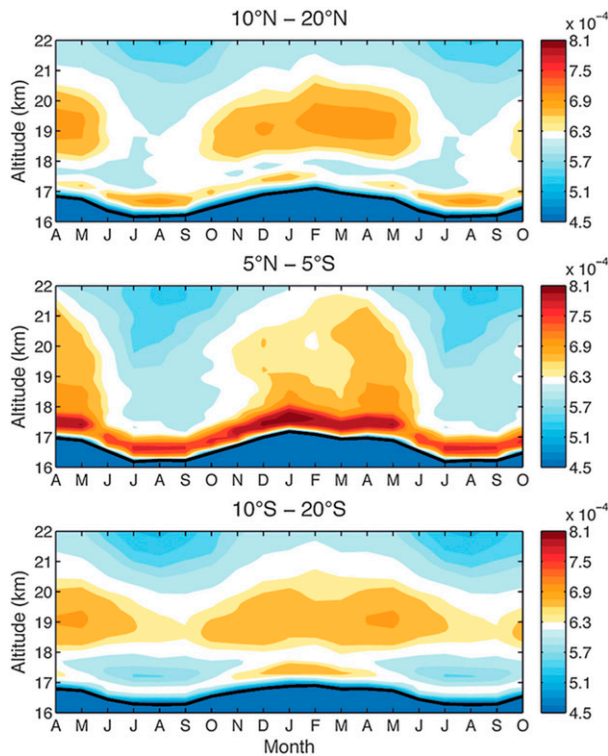


FIG. 4. Seasonal cycle of static stability structure (square of buoyancy frequency N^2) in the UTLS over three different tropical latitude bands [(top) $10^\circ\text{--}20^\circ\text{N}$, (middle) $5^\circ\text{N--}5^\circ\text{S}$, and (bottom) $10^\circ\text{--}20^\circ\text{S}$], derived from *CHAMP* measurements for the period from April 2002 to March 2008. The thick black solid line denotes monthly mean lapse-rate tropopause (LRT) height. Monthly means of N^2 have been computed in LRT-relative coordinates. Values below $4.5 \times 10^{-4} \text{ s}^{-2}$ are not contoured (Grise et al. 2010).

secondary thin static stability maximum just below the zero wind line associated with the descending westerly shear phase of the QBO and have found the enhanced TIL strength associated with deep convective outflow and equatorial waves. Noersomadi et al. (2019) have quantified TIL strengthening due to enhanced convective activity associated with the MJO, ENSO, and monsoon circulations.

4. Clouds and convection

The high vertical resolution, insensitivity to weather conditions and the global coverage make RO well suited to study temperature changes due to extreme weather and volcanic clouds. These phenomena were not the objectives of the first RO missions, but quickly became one of the focuses when scientists understood the importance of the high vertical resolution to study cloud structure and dynamics.

a. Deep convection

During convective development, the environmental temperature decreases from the surface to the midtroposphere with a lapse rate close to the climatological temperature

profile. In the cloud, the lapse rate increases and the temperature reaches a minimum near the cloud-top height, where a rapid inversion may reestablish the standard lapse rate (Biondi et al. 2012; Bonafoni and Biondi 2016). The largest negative temperature anomaly corresponds to the cloud-top height of the deepest convection (reaching heights greater than 17 km) with the magnitude decreasing for lower cloud-top heights down to 15 km (Paulik and Birner 2012). When deep convection does not reach the standard tropopause height, the presence of the cloud can create a secondary tropopause associated with the inversion at the cloud top (Biondi et al. 2012; Shi et al. 2017) as shown in Fig. 5. In particular cases, such as deep convection developing in the western Pacific during an active MJO, a thermal vertical dipole appears with large horizontal scale characterized by warming in the upper troposphere and cooling near the tropopause and lower stratosphere, which enhances dehydration of the lower stratosphere (Kim et al. 2018). However, the temperature anomalies in the lower stratosphere can sometimes differ in case of tropopause-penetrating convection or nonpenetrating convection (Xian and Fu 2015) and in different regions of the globe (Johnston et al. 2018). Collocation with rainfall measurements from the Tropical Rainfall Measuring Mission (TRMM) has shown that tropopause-penetrating convection is characterized by warm anomalies in the midtroposphere, cold anomalies at the tropopause and lower stratosphere with a rapid lift of the LRT height. In contrast, nonpenetrating convection shows cooling at the tropopause and warming in the lower stratosphere (Xian and Fu 2015; Johnston et al. 2018).

A diurnal temperature anomaly due to the nonmigrating tides and overshooting turrets is usually evident during strong convection (Khaykin et al. 2013; Johnston et al. 2018) with amplitudes proportional to the strength of the convection and more evident over land in the southern tropics (Khaykin et al. 2013). Land convection cools the lower stratosphere more than ocean convection (Johnston et al. 2018). The temperature of the lower stratosphere in summer over land shows a diurnal cycle collocated with the most intense convective activity, with afternoon cooling also corresponding to the maximum frequency of overshooting in the area.

b. Tropical cyclones

The use of RO also allows improved understanding of tropical cyclone (TC) thermal structure, including the differences between TCs developing in different areas (Bonafoni et al. 2019). Although the RO profiles have a horizontal averaging scale of approximately 250 km, most of the information in the RO profile represents smaller horizontal scales closer to 50 km (Anthes et al. 2000), and hence capture an important part of the TC temperature anomalies. The RO profiles confirm the already well-known TC warm core, but also highlight the cold TC cloud top (Biondi et al. 2011a) and the presence of a double tropopause in some specific cases (Biondi et al. 2011b). The collocation of RO profiles with radiosonde profiles during TCs (Biondi et al. 2013) shows a cooling at the TC cloud-top height with a strong inversion layer over the cloud top. Rivoire et al. (2016) showed that the cooling at the tropopause level precedes the formation of the TC warm core and

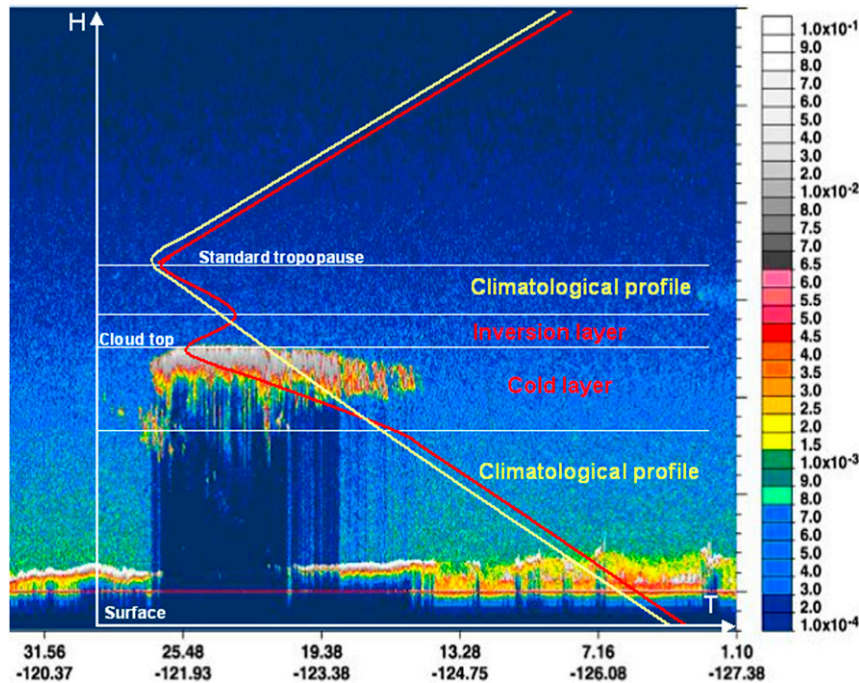


FIG. 5. Atmospheric thermal structure during severe convection, estimated by GNSS RO. The yellow line shows the climatological temperature profile, and the red line shows the usual temperature profile during the deep convection events. The background shows the attenuated backscatter of a squall line from CALIOP (Biondi et al. 2012; <https://creativecommons.org/licenses/by/4.0/>; no changes were made).

speculated about a positive feedback for the intensification of the storm.

A comprehensive study by Biondi et al. (2015) characterized the TC thermal structure by ocean basin and intensity collocating the RO profiles with the TCs' center coordinates in a time window of 6 h and a space window of 600 km. The results showed different features according to the ocean basins (see

Fig. 6). The TC cloud top in the Southern Hemisphere ocean basins is usually colder than in the Northern Hemisphere and the anomaly remains negative up to an altitude of 25 km. The TCs in the Northern Hemisphere ocean basins, on the other hand, show a positive temperature anomaly above the cloud top. The double tropopause characterizes the TC at all intensities in all the ocean basins even though it is more frequent at extratropical latitudes.

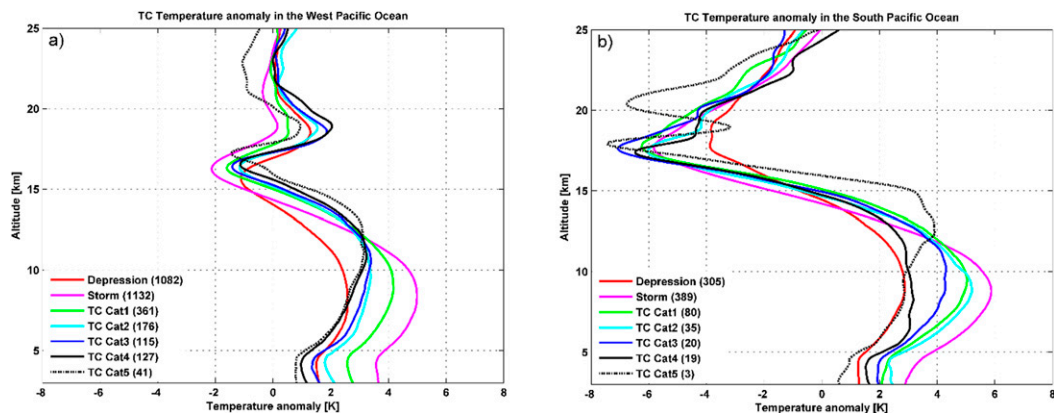


FIG. 6. Mean temperature anomalies for different TC storm categories shown for the (a) western Pacific Ocean and (b) South Pacific Ocean. Numbers in parentheses denote the numbers of observations. The RO profiles are collocated with the TC center coordinates in a time window of 6 h and a space window of 600 km (Biondi et al. 2015; <https://creativecommons.org/licenses/by/4.0/>; no changes were made).

Some studies limited to the north Indian Ocean (Ravindra Babu et al. 2015; Ratnam et al. 2016) evaluated the impact of TCs on the tropopause parameters at different distances from the TC center. They found the largest effect on the tropopause height and temperature within 500 km from the center. The tropopause height was a minimum over the center and gradually increased outward, while the tropopause temperature increased outward from the center to beyond 500 km. The closest profiles to the TC centers also show multiple tropopauses, confirming the results of previous studies (e.g., Biondi et al. 2015).

A comprehensive archive of collocations between TCs and RO profiles is provided by Lasota et al. (2020).

c. Volcanic cloud impacts

Wang et al. (2009) were the first using RO data for studying the impact of the Mount Chaiten 2008 eruption on atmospheric temperature. Volcanic clouds in the UTLS modify the thermal layer structure immediately after the eruption, producing a cooling at the cloud-top height (Okazaki and Heki 2012; Biondi et al. 2017; Cigala et al. 2019). The buoyancy perturbation produced by the eruption pushes up the tropopause level relative to the standard atmosphere in the same area and season (Biondi et al. 2017; Prata et al. 2020) and creates conditions in which the altitude distance between the CPT and the LRT increases by a few kilometers (Prata et al. 2020) instead of a few hundred meters as in standard conditions. The volcanic effect in the UTLS can be different for different eruptions: Nabro in 2011 produced a quick warming of the lower stratosphere (Biondi et al. 2017), whereas Anak Krakatau in 2018 warmed the upper troposphere and cooled the lower stratosphere (Prata et al. 2020).

It has been recently suggested that even relatively small volcanic eruptions can impact the climate (Solomon et al. 2011). Mehta et al. (2015) used 10 years of RO data (2001–10) to estimate the impact of minor volcanic eruptions on the UTLS thermal structure. They found a significant volcanic signal in the residual temperature of the Soufriere Hills 2006 and Tavurvur 2006 eruptions with a warming in the lower stratosphere. No significant impact was found from other eruptions, as impacts of smaller eruptions are difficult to quantify in the background of natural variability. Stocker et al. (2019) used vertically high resolved aerosol observations together with RO to quantify volcanic imprints on stratospheric temperature. They found robust warming signals in the lower stratosphere, corresponding to the Tavurvur 2006, Merapi 2010, Nabro 2011, and Calbuco 2015 eruptions. In the midstratosphere, cooling signals for some eruptions appear, possibly due to uplift of ozone poor air.

5. Gravity waves

Gravity waves (GWs) have scales too small to be realistically described by data assimilation in global reanalysis datasets. However, collectively they contribute substantially to the global circulation momentum budget, particularly at levels in

the upper troposphere and above (Alexander and Ortland 2010; Geller et al. 2013). GW temperature anomalies also lower the cold-point temperature of air rising through the TTL, modulating cirrus cloud occurrences and lowering the concentration of water vapor entering the stratosphere (Jensen and Pfister 2004; Kim and Alexander 2015). While GW breaking and cloud seeding processes are localized in space and time, the collection of many GW events has global effects on general circulation and surface temperature (Richter et al. 2010; Kim and Alexander 2015). Therefore, while research work on a wide variety of GW processes requires detailed local measurement of wave properties such as temperature anomalies, wavelengths, phase speeds, and momentum fluxes, global coverage is also needed to address these issues.

RO temperature profiles contain information on short-vertical-scale GWs. Many early studies attempted to isolate GWs from the large-scale temperature structure by performing a polynomial fit to individual RO temperature profiles to define a “background temperature profile” and then interpreting the residual temperature anomalies as those caused by GWs (de la Torre et al. 2004; Ratnam et al. 2004; de la Torre et al. 2006; Alexander et al. 2008a; Schmidt et al. 2008a; de la Torre et al. 2010; Luna et al. 2013; Chane Ming et al. 2014; Nath et al. 2015). This definition of background temperature allows for retrieval of information on short-vertical-scale temperature anomalies, which include all waves with a vertical wavelength typically in the range ~ 2 –10 km (Steiner and Kirchengast 2000; Tsuda et al. 2004, 2011; Wright et al. 2011).

Tsuda et al. (2000) mapped the variance of small-vertical-scale temperature anomalies with this method using GPS/MET RO temperature retrievals. The global map of November–February averaged wave potential energy (PE) at 20–30 km derived from these temperature anomalies showed a clear peak in energy at low latitudes, as well as a winter season enhancement compared with the summer season at extratropical latitudes. Tsuda et al. (2000) suggested that the tropical peak shows waves generated by convection and recognized that these small-vertical-scale anomalies could include contributions from global-scale tropical wave modes as well as smaller-scale GWs. Indeed, Holton et al. (2001) subsequently found global-scale Kelvin waves with very short vertical wavelengths of 3–4.5 km and temperature amplitudes up to 6 K. Alexander and Ortland (2010) found tropical Rossby and mixed Rossby–GW (MRGW) modes with vertical wavelengths as short as 4 km and amplitudes near 2 K. de la Torre et al. (2006) performed an analysis similar to Tsuda et al. (2000), but reported short-vertical-wavelength (< 10 km) variances in multiple years of SAC-C and CHAMP RO temperature profiles. The same tropical enhancement is evident, but with a clear interannual variation related to the QBO in tropical winds. These results are consistent with a mixture of global-scale tropical waves and smaller-scale GWs interacting with QBO wind shear zones, since vertical wavelengths grow small as waves approach a critical level where the wave phase speed equals the wind speed.

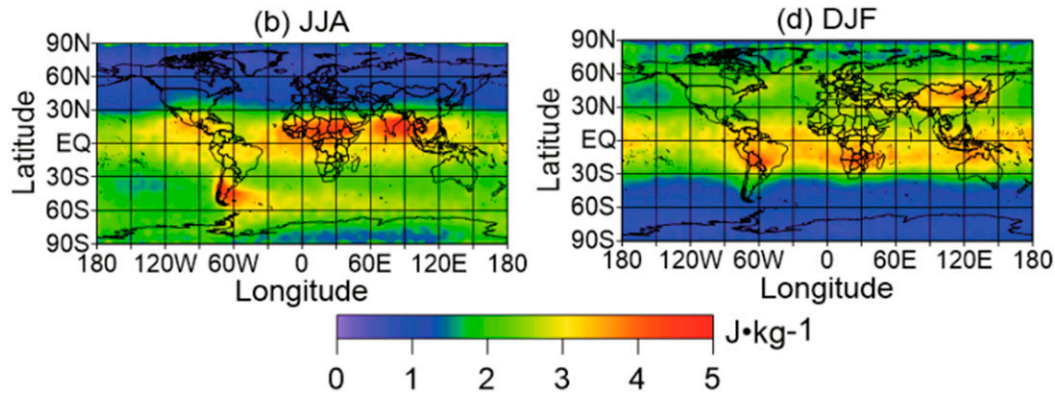


FIG. 7. Potential energy maps (J kg^{-1}) averaged over 2006–13 for altitudes 20–30 km in the solstice seasons derived from RO measurements after removal of planetary-scale waves, showing clear relation to deep convection and orographic sources [reprinted by permission from Springer Nature Customer Service Centre GmbH: Springer Nature, *Advances in Atmospheric Sciences* (<https://www.springer.com/journal/376/>); Xu et al. 2018; copyright 2018].

GWs may develop very long vertical wavelengths when stratospheric winds become strong enough. A simplified form of the GW dispersion relation shows this:

$$|m| = N/|U - c|,$$

where m is the vertical wavenumber [$2\pi/(\text{vertical wavelength})$], N is the buoyancy frequency, U is the horizontal zonal wind speed upstream of the direction of wave propagation, and $U - c$ is the intrinsic phase speed. The equation indicates that, with $N \approx 0.02 \text{ s}^{-1}$, vertical wavelengths may exceed 10 km (the limit often imposed by a vertical fit to define a “background temperature”) whenever the intrinsic phase speed exceeds 32 m s^{-1} . Zonal winds commonly exceed 32 m s^{-1} during midwinter. In the tropics, studies applying a vertical polynomial fit to define the background temperature for RO will include planetary-scale waves, and may exclude important convectively generated GW signals with high phase speeds, particularly those propagating upstream against QBO winds where $|U - c|$ is large. Relating vertically high-pass-filtered PE to wave sources has sometimes indicated correlations with tropical deep convection (Kawatani et al. 2003; Ratnam et al. 2004; Chane Ming et al. 2014) or topography (Noersomadi and Tsuda 2016; Rapp et al. 2018). However, quantitative information about wave properties that could improve parameterization of GW effects on circulation has been difficult to acquire with these methods (Alexander 2015). The parameterizations need gravity wave momentum fluxes, which require determination of the three-dimensional structure of gravity waves to derive it from temperature measurements (Ern et al. 2004).

One estimate of the contributions to the short-vertical-wavelength signal of GWs versus longer-period planetary-scale waves appears in Kim and Alexander (2015). Analyzing tropical radiosondes, they found that vertical wavelengths including all wave types in the TTL peak at $\sim 4 \text{ km}$, but only $\sim 1/4$ of the temperature variability is contributed by GW frequencies, while $\sim 3/4$ is contributed by waves with periods longer than 3 days. Comparing COSMIC and radiosonde subseasonal-to-interannual variations in wave-induced CPT

variability showed that the two datasets were quantitatively very similar, suggesting that RO captures most or all the important short vertical wavelength waves contributing to CPT variability.

Other methods for defining the large-scale, zonal-mean, and planetary-scale wave temperature structure have since been developed, and can be applied to improve the separation of GW signals from other planetary-scale waves, while also avoiding the low-pass vertical filtering that was eliminating many important long-vertical-wavelength GWs. Horinouchi and Tsuda (2009) studied unique sets of near-instantaneous quasi-linear groupings of COSMIC temperature profiles during the first December–February following the satellite launch (2006–07). Focusing on groupings at midlatitudes in boreal winter, they were able to identify propagation directions, and found a preference for northward over southward propagation indicating more wave sources at lower latitudes. J.-E. Kim et al. (2016) found clear relationships between wave-induced cooling and thin cirrus occurrence. Studies comparing RO density perturbations to temperature perturbations in Šácha et al. (2014) and Pišoft et al. (2018) showed that both methods represent a high-pass filter eliminating vertical wavelengths of $< 8 \text{ km}$.

A number of studies used RO temperatures to define a background for analyses of residual variance as GWs (Randel and Wu 2005; Wang and Alexander 2009, 2010; McDonald 2012; Alexander et al. 2013; Faber et al. 2013; Alexander 2015; Schmidt et al. 2016a; Xu et al. 2018). These methods appropriately distinguish GWs and planetary-scale waves by horizontal wavelength and/or period rather than by vertical wavelength. With this method, Xu et al. (2018) showed that GW PE (Fig. 7) does not peak directly over the equator but shifts to the tropical summer hemisphere over continental landmasses where convection is strongest.

Success in identifying GW horizontal wavelengths, propagation directions, and momentum fluxes have been derived by removing planetary-scale waves, followed by selection of special subsets of RO profiles that are close in space and time. Alexander (2015) and Schmidt et al. (2016a) used triads of

limb-sounding temperature profiles that are close in space and time to retrieve three-dimensional properties of GWs, dramatically improving estimates of GW horizontal wavelengths and momentum fluxes. Alexander (2015) combined pairs of high-resolution dynamics limb sounder (HIRDLS) profiles together with a nearby COSMIC profile, while Schmidt et al. (2016a) used RO from multiple missions to find close triads. Both obtained very similar zonal-mean values of GW momentum fluxes that peak in the winter extratropics. Schmidt et al. (2016a) considered line of sight angle in their triad analysis, and de la Torre et al. (2018) highlighted potential effects of the slant angle of RO profiles on horizontal wavelength retrievals. These effects are particularly important for short-horizontal-wavelength GWs, and relatively less important for the longer-horizontal wavelengths (>250 km) that are typically retrieved by RO and other limb-sounding methods.

Future higher density RO temperature profile measurements can be exploited to improve knowledge of GW properties, but the optimal measurement density requires multiple simultaneous closely spaced profiles. RO observed from long duration stratospheric balloon platforms (Haase et al. 2018) are expected to probe the resolution limits of the RO technique for tropical GWs.

6. Atmospheric planetary waves

a. Atmospheric thermal tides

Atmospheric thermal tides are persistent planetary-scale global oscillations, with periods of some integer fractions of a solar day. They are mostly excited by the absorption of solar radiation, latent heat release, or nonlinear wave-wave interactions. Tides that are generated in the lower atmosphere propagate upward with exponential growth in amplitude, dominate the motion of the mesosphere, and deposit their energy and momentum in the lower thermosphere (Hagan and Forbes 2002, 2003). Tides can be separated into two components: migrating and nonmigrating. Migrating tides are sun-synchronous, moving westward with the apparent motion of the sun, while nonmigrating tides do not. Measuring the tides from the source regions (close to the UTLS) is essential for understanding, monitoring, and predicting changes in the whole atmosphere.

However, our observational picture is based on limited data: (i) tidal amplitudes in the UTLS are relatively small (~ 0.5 K), which requires highly accurate measurements; (ii) tidal analysis is best for observations with full local-time sampling, which is generally not achievable from ground-based observations (which cannot separate the migrating and nonmigrating tides) or a single satellite measurement (which often has specific local-time sampling).

RO data have been used to study tides due to their high quality in the UTLS (Zeng et al. 2008; Pirscher et al. 2010; Xie et al. 2010; Khaykin et al. 2013; Sakazaki et al. 2015). Zeng et al. (2008) first used CHAMP RO dry temperature at 10–30 km from 2001 to 2005 to estimate the migrating diurnal tidal structures in the tropics. The problem of local-time sampling

from a single satellite has been overcome by considering the slow local-time drift of CHAMP and merging multiyear data. Pirscher et al. (2010) advanced the study by using COSMIC data, which sampled all local times within one month equatorward of 50°N/S. Both studies revealed that diurnal amplitudes in temperature increase with altitude and reach ~ 1 K at 30 km in the tropics but exhibit strong annual and latitudinal variations. These variations are clearly linked to the movement of the intertropical convergence zone. The tides propagate upward with a vertical wavelength of about 20 km. Khaykin et al. (2013) found differences of diurnal tidal variations between land and ocean in the lowermost stratosphere, which are associated with nonmigrating tides generated by the land-ocean contrast and/or the local effects of deep overshooting convection. Sakazaki et al. (2015) extracted tropical nonmigrating tides that are excited by diabatic heating over Africa and South America and propagate zonally away from their sources.

b. Equatorially trapped waves

Planetary-scale disturbances propagating parallel to the equator have been observed since the 1960s (Yanai and Maruyama 1966; Wallace and Kousky 1968) and theoretically understood as the equatorially trapped waves (Matsuno 1966; Lindzen 1967). In the troposphere, the waves that are primarily forced by deep tropical convection are convectively coupled and therefore visible in OLR data (Wheeler and Kiladis 1999). Transient deep convection also forces equatorial waves in the UTLS, but these waves have faster phase speeds that represent the remote response (Garcia and Salby 1987). Corresponding temperature perturbations can be observed throughout the UTLS (Tsai et al. 2004; de la Torre et al. 2004). These waves are important as they drive the QBO, lower the tropical CPT temperature, and modulate the transport of trace constituents and water vapor from the troposphere into the lower stratosphere (Kim and Alexander 2015).

Understanding of equatorially trapped waves has advanced through high-temporal- and spatial-resolution satellite data. RO-focused analyses have been complemented by analyzing data from a range of satellite instruments including Sounding of the Atmosphere Using Broadband Emission Radiometry (SABER) (Ern et al. 2008) and HIRDLS (Alexander and Ortland 2010). Vertical resolution of RO data is higher than that of SABER and similar to HIRDLS. While comparisons with radiosonde measurements revealed a limited representation of waves with short vertical wavelengths in RO data (Kim and Alexander 2015), wave structures and their propagation can be studied globally with RO data.

RO data sampling is optimal to resolve eastward propagating Kelvin waves. These waves are symmetric about the equator and propagate eastward in the stratosphere in regions with easterly background winds (e.g., Sato and Dunkerton 1997). Wavenumbers range from $k = 1$ to 5, periods from approximately 3 to 30 days, and vertical wavelengths from 2 to 24 km (phase speeds from 7 to 75 m s^{-1}) (Alexander and Ortland 2010). Kelvin waves with zonal wavenumbers of one and two were resolvable in the coarser-resolution CHAMP data (Tsuda et al. 2006), which revealed wave amplitudes of 2–4 K,

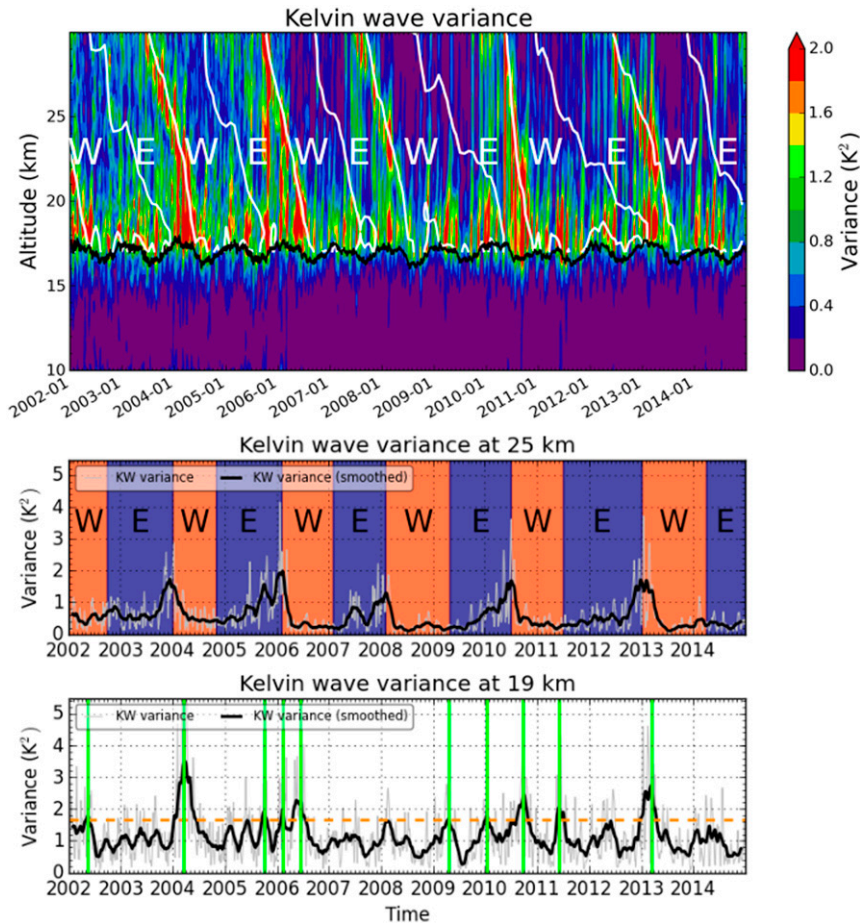


FIG. 8. Time series of Kelvin wave temperature variance (K^2) from January 2002 to December 2014 (top) as a function of altitude, (middle) at 25 km, and (bottom) at 19 km. The thick black line in the top panel indicates the LRT, thin white contour lines indicate zero zonal wind speed above Singapore, and E and W refer to easterly and westerly wind (orange and blue background in the middle panel). Green lines in the bottom panel indicate points of time with smoothed Kelvin wave variance outside of one standard deviation ($1.66 K^2$, indicated by the dashed yellow line) (Scherrlin-Pirscher et al. 2017a; <https://creativecommons.org/licenses/by/4.0/>; no changes were made).

vertical wavelengths of 4–8 km, and the characteristic eastward phase tilt with height (Tsai et al. 2004; Randel and Wu 2005).

The large increase in the number of RO profiles from the COSMIC satellite constellation enabled studies of Kelvin waves with higher zonal wavenumbers and shorter periods. Alexander et al. (2008b) observed higher wavenumber Kelvin waves with periods of about 5 days and maximum amplitudes of 2 K. Fast Kelvin waves observed by COSMIC had wave amplitudes smaller than 1.2 K and periods of less than 10 days.

The Kelvin wave periods reported in these RO studies are consistent with theory (i.e., wave periods confined within the region of large power in the symmetric wavenumber-frequency power spectra). The RO observations of wave periods are consistent with outgoing longwave radiation observations, which by definition are coupled to the top of the generating

cloud systems (Wheeler and Kiladis 1999); and the RO-derived periods and temperature amplitudes are consistent with radiosonde observations (e.g., Wallace and Kousky 1968; Shimizu and Tsuda 1997; Suzuki et al. 2013).

Kelvin waves dominate subseasonal variability in the tropical tropopause region (Kim and Son 2012) and their activity increases in the upper troposphere when deep, transient convection is present (Randel and Wu 2005). In the TTL the seasonal structures and interannual variability of Kelvin wave activity are dominated by the background wind fields and tropospheric convection likely plays a minor role (Flannaghan and Fueglistaler 2013). However, relationships between Kelvin wave activity and wind near the tropopause are still not clear as shown in Fig. 8, where peaks of Kelvin wave activity are not only observed during the westerly shear phase of the QBO (top panel) but are irregularly distributed in time (bottom panel) (Scherrlin-Pirscher et al. 2017a).

In the lower and middle stratosphere, Kelvin wave activity is strongly modulated by the QBO with enhanced activity observed during the descending westerly wind shear QBO phase (Randel and Wu 2005; Ratnam et al. 2006; Scherllin-Pirscher et al. 2017a). Kelvin waves propagate upward in QBO easterlies, with a vertical group velocity proportional to their intrinsic phase speed squared $(U - c)^2$. In upper-level regions of westerly shear the waves slow down and amplify (hence the large temperature variance), and thermal damping results in momentum deposition and eastward acceleration of the zonal flow.

RO data have been used to validate Kelvin wave activity of general circulation models and atmospheric reanalyses (Kawatani et al. 2009; Flannaghan and Fueglistaler 2013). It was found that wave activity in the TTL increased in the ERA-Interim reanalysis with the assimilation of COSMIC RO data (Flannaghan and Fueglistaler 2013).

Westward-moving MRGWs are antisymmetric about the equator and have periods of less than 5 days. While individual phases of MRGWs propagate westward, the wave packets propagate eastward. The sporadic nature of MRGWs contributes to their low variance in wavenumber-frequency spectra, yet they are at times clearly visible in the data (Alexander et al. 2008b; Alexander and Ortland 2010). There remain very few RO studies of MRGWs, although Alexander et al. (2008b) showed MRGWs with amplitudes around 1 K that vanished once the background mean flow became westward.

7. Intraseasonal-to-interannual atmospheric modes of variability

In addition to fast equatorial waves and various tropical phenomena in the troposphere and stratosphere, temperatures in the tropical UTLS reveal a wide range of variabilities spanning intraseasonal through interannual time scales. Owing to the high accuracy and fine vertical resolution of RO, these sources of atmospheric variability are better quantified on an observational basis.

a. Intraseasonal variability

The intraseasonal variation in the tropical UTLS is mostly related to the equatorial waves (Wallace and Kousky 1968; Tsuda et al. 1994) and the MJO (Kiladis et al. 2001). As described in the previous section, detailed features of intraseasonal variability related to the equatorial waves are well captured by RO due to its high vertical resolution and global coverage (e.g., Alexander et al. 2008b; Kim and Son 2012; Scherllin-Pirscher et al. 2017a).

The MJO is another important source of intraseasonal variability in the tropics. It is generally characterized by organized mesoscale convection in the tropics propagating from the Indian Ocean to the central Pacific (around the date line, Zhang 2005). The circulation and convective heating of the MJO produces a unique temperature anomaly structure showing tropospheric warming covered by a thin layer of cooling near the tropopause (Kiladis et al. 2001; also shown in Fig. 9). Particularly the near-tropopause cooling has a strong temperature anomaly of $\sim 2\text{--}4\text{ K}$ in a narrow vertical depth of

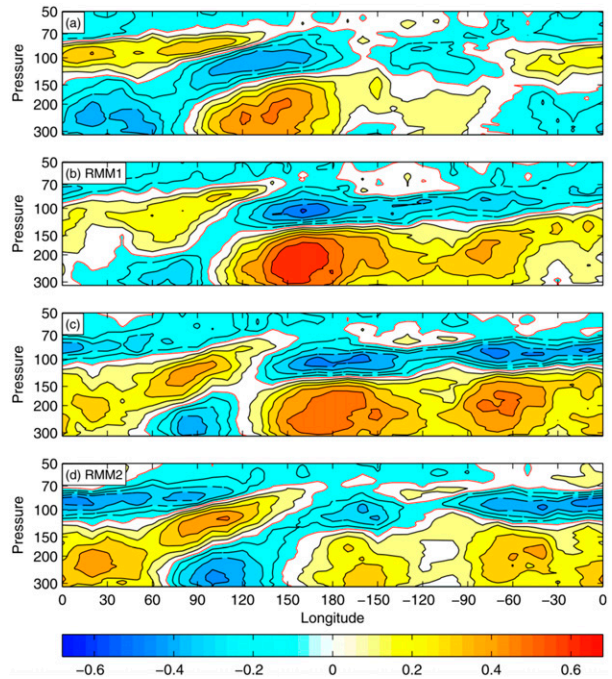


FIG. 9. RO-based temperature anomalies in the deep tropics (5°N/S) correlated with the real-time multivariate Madden-Julian oscillation (RMM) indices. This represents one-half of an MJO cycle (Virts and Wallace 2014).

2–3 km, which impacts water vapor content and cirrus clouds in the tropical tropopause layer (Virts and Wallace 2014; Kim et al. 2018). The temperature anomaly increases the static stability above the tropopause and affects the strength of the tropopause inversion layer. The detailed features are clearly captured by RO measurements and they show coherent features with satellite composition and cloud measurements during MJO events (Kim and Son 2012; Virts and Wallace 2014; Noersomadi et al. 2019). Furthermore, the tropospheric and stratospheric temperature anomalies propagate slowly to the east following the organized convection in the MJO (Fig. 9). These transient characteristics are observed well by RO data because of its enhanced sampling rate and spatial coverage over the tropics (e.g., Tian et al. 2012; Zeng et al. 2012). Recent work has highlighted that MJO UTLS structure is strongly modulated by the QBO (Hendon and Abhik 2018).

b. Annual cycle

The annual cycle is the dominant source of variability in the tropical UTLS over altitudes $\sim 16\text{--}22\text{ km}$ with the maximum annual difference of 8 K at $\sim 18\text{ km}$ (Kim and Son 2012; Randel and Wu 2015). Particularly, a significant temperature variation is caused by the Brewer–Dobson circulation (BDC) inducing more vigorous tropical upwelling (and adiabatic cooling) in the tropical stratosphere during the boreal winter than in the boreal summer (Fueglistaler et al. 2009). This temperature variation is further amplified by local radiative forcing from ozone and water vapor (Fueglistaler et al. 2011;

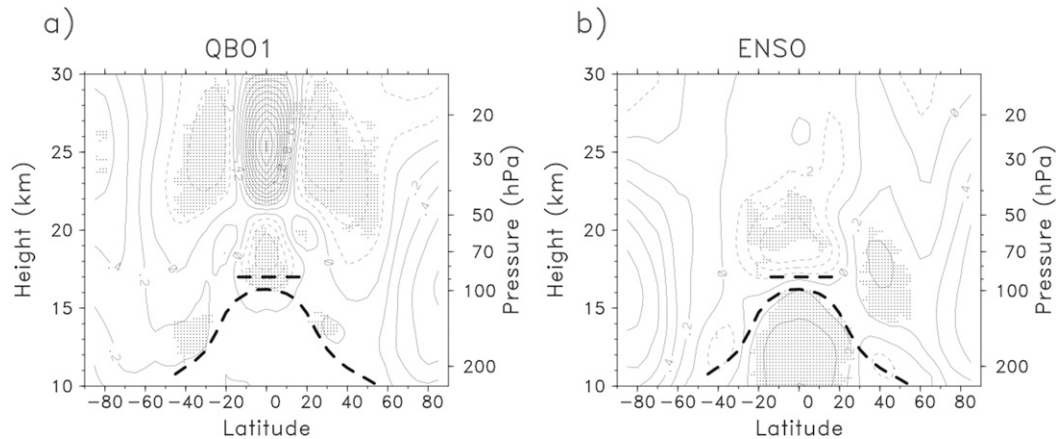


FIG. 10. Zonal-mean RO temperature signals for (a) QBO and (b) ENSO climate indices derived from regression over 2002–14. QBO1 is the first principal component of QBO variability described by Wallace et al. (1993), and ENSO is based on the multivariate ENSO index (MEI; <https://psl.noaa.gov/ens/mei/>). Contours interval is 0.2 K, with negative values dashed. Shading shows statistically significant values at 99% level. The heavy dashed lines denote the thermal and cold-point tropopauses (Randel and Wu 2015).

Ming et al. 2017). This temperature variability is accurately quantified at the tropopause and in the lower stratosphere by RO measurements (Schmidt et al. 2004; Son et al. 2011; Kim and Son 2012; Rieckh et al. 2014). Also, RO, with its fine vertical resolution, revealed that the annual cycle of temperature is maximized in the lowermost stratosphere (e.g., Randel et al. 2003; Schmidt et al. 2004; Kim and Son 2012), which became the key observational evidence supporting the importance of the lower branch of the BDC for driving the annual cycle in the tropical UTLS (Ueyama et al. 2013; J. Kim et al. 2016).

With an increased sampling of temperature profiles from the COSMIC mission, spatial structures of the UTLS temperature were also examined for different seasons, revealing regional details of seasonal anomalies in near-tropopause temperature and inversion layer (Nishi et al. 2010; Grise et al. 2010; Kim and Son 2012; Scherllin-Pirscher et al. 2017a). For example, RO clearly captures quasi-stationary cold anomalies located over the western Pacific in boreal winter and South Asia in boreal summer related to seasonal migration of deep convection. A frequent upper tropospheric inversion is also observed over the equatorial Indian Ocean during boreal summer (Nishi et al. 2010). Newton and Randel (2020) have shown that these quasi-stationary inversions are a climatological feature, linked to transient convectively forced Kelvin waves that are Doppler shifted in the background UTLS easterly winds of the Asian monsoon anticyclone.

c. Interannual variability

Interannual variability in the tropical UTLS is associated with tropospheric and stratospheric processes. The QBO is a well-known source of stratospheric variability that is identified as alternating westerly and easterly winds in the deep tropics (within 10°N/S; Baldwin et al. 2001). A warm (cold) anomaly accompanies westerly (easterly) shear layers due to thermal-wind balance in the tropics, and the temperature anomalies

affect the tropical UTLS down to the tropopause region with an approximate 28-month cycle. The maximum QBO-related temperature anomalies measured by RO are approximately ± 4 K over altitudes of ~ 22 –31 km (Fig. 10), which is consistent with the radiosonde observations at Singapore (Baldwin et al. 2001). Although the amplitude of the temperature variation diminishes downward, its impact near the CPT is still crucial as it modulates the amount of the stratospheric water vapor (Randel et al. 2004; Randel and Park 2019). The temperature impact has been clearly detected in the lower stratosphere and at the tropopause by early records of RO (e.g., Randel et al. 2003; Schmidt et al. 2005). The QBO-induced temperature variation at the cold point appears uniformly in the deep tropics (15°N/S), and it is quantified as approximately ± 0.5 K by longer RO records (e.g., Son et al. 2017; Wilhelmson et al. 2018).

Another source of interannual variability in the tropical UTLS originates from ENSO-related changes in organized convection (Yulaeva and Wallace 1994). Notably, a positive phase of the ENSO enhances convection in the tropical central to eastern Pacific while suppressing it over the western Pacific (vice versa in the negative phase). This strongly influences the three-dimensional UTLS temperature structure, including a large longitudinal shift in seasonal temperature anomalies and a zonal-mean response (e.g., Calvo Fernández et al. 2004; Scherllin-Pirscher et al. 2012). The zonal-mean influence of positive ENSO is warming in the tropical upper troposphere and cooling in the lower stratosphere (Fig. 10b) with maximum zonal-mean response approximately 3 months after ENSO forcing (Randel et al. 2009; Lackner et al. 2011b; Scherllin-Pirscher et al. 2012). The most pronounced zonal-mean tropospheric warming (8–15 km) reaches up to 2 K. Longitudinal UTLS response to ENSO effects occur more rapidly (within 1 month) and feature maximum amplitude in the upper troposphere (near 11 km) and with opposite polarity in a shallow layer near the tropopause (Scherllin-Pirscher et al. 2012).

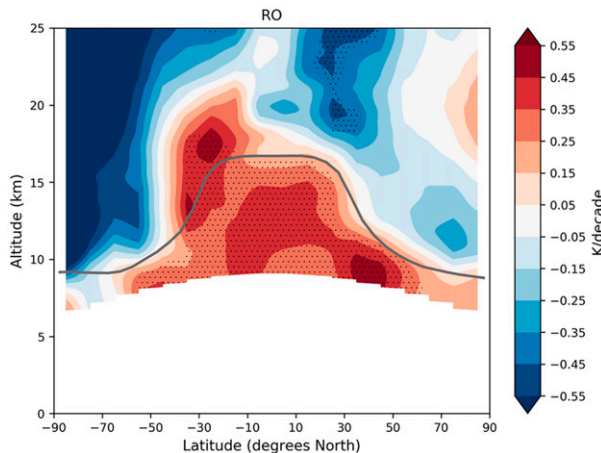


FIG. 11. Altitude vs latitude-resolved trends (K decade^{-1}) in RO dry temperature over 2002–18. Stippling indicates trend values that are significant at the 95% confidence level (Steiner et al. 2020b; <https://creativecommons.org/licenses/by/4.0/>; no changes were made).

ENSO dynamics is also associated with a higher number of double tropopauses during the negative ENSO phase, which is clearly visible in the tropical eastern Pacific (Wilhelmsen et al. 2020).

In addition to the QBO and ENSO, interannual variations in the BDC (Randel and Wu 2015) and enhanced MJO convection during the easterly phase of the QBO (Son et al. 2017) contribute to the interannual temperature variability in the tropical UTLS by directly affecting temperature or modulated convection in the tropics. The high-resolution temperature observations from RO significantly contribute to understanding the dynamic mechanisms involved in these processes.

8. Climate applications

a. Climate monitoring and benchmarking

RO has been identified as a key component for the Global Climate Observing System (GCOS) owing to its potential as a climate benchmark measurement (GCOS 2011, 2016). Benchmark measurements can be related to absolute standards and may be repeated at any subsequent time with precise comparability (Goody et al. 1998, 2002), such that the accuracy of the record archived today can be verified by future generations. Traceability to standards of the International System of Units (SI) is the foundation for benchmark measurements (Leroy et al. 2006b; Ohring 2007). For RO, the fundamental measurement is the GNSS signal phase change as function of time, based on highly precise and stable atomic clocks (see section 2).

RO observations can be assimilated without bias correction in numerical weather prediction models. Most modern reanalyses assimilate RO observations producing more consistent temperature analyses in the upper troposphere and stratosphere (e.g., Fujiwara et al. 2017; Hersbach et al. 2020).

For climate signal detection, the uncertainty in the observations must be smaller than the expected change signals (Ohring et al. 2005; Bojinski et al. 2014). In the UTLS, RO observations are of highest accuracy and the structural

uncertainty arising from different processing schemes is smallest (see section 2). The RO record from 2002 to the present is found suitable for trend detection (Steiner et al. 2020a). The structural uncertainty of temperature between 8 and 25 km altitudes is $<0.05 \text{ K decade}^{-1}$ for the global mean and $<0.1 \text{ K decade}^{-1}$ for individual latitude bands, conforming to GCOS requirements.

Yuan et al. (1993) were among the first who suggested the use of RO for trend detection. By simulating the propagation of GPS signals in a climate model with doubled carbon dioxide concentration, they found an increase in the signal phase path. Melbourne et al. (1994) and Ware et al. (1996) further stated that RO could detect trends over short time periods. More quantitatively, Leroy et al. (2006a) estimated climate change signal detection times of only 7–13 years for a scenario with $1\% \text{ yr}^{-1}$ growth in carbon dioxide.

For the same forcing scenario, clear signals of bending angle trends with detection times of 10–16 years were shown in climate simulation experiments (Ringer and Healy 2008). Vedel and Stendel (2003), Stendel (2006), and Leroy et al. (2006a) investigated the value of RO geopotential height and refractivity for climate studies. The complementary sensitivity for monitoring the UTLS was demonstrated with observing system simulation experiments for a medium emission scenario (Steiner et al. 2001; Foelsche et al. 2008b) and climate change indicators (Lackner et al. 2011a).

b. Detection of short-term trends

The detection of trends in short-term records requires appropriate accounting of natural variability. Steiner et al. (2009) were the first to demonstrate the trend detection capability of actual RO temperature observations using GPS/MET and CHAMP observations from 1995 to 2008. They showed an emerging warming trend in the tropical troposphere and a significant cooling trend in the tropical lower stratosphere.

In an optimal fingerprinting study, Lackner et al. (2011b) investigated climate change patterns in several RO variables for the period of 2001–10. They detected emerging trend signals in geopotential height (90% confidence level) and temperature (95% confidence level). In the tropics, a warming of $\sim 0.3 \text{ K decade}^{-1}$ was detected in the upper troposphere and a cooling of $\sim 0.6 \text{ K decade}^{-1}$ in the lower stratosphere. Warming of the tropical tropopause layer was confirmed by Wang et al. (2015). The most recent study of Steiner et al. (2020b) gives an update on UTLS temperature trends from a range of observations. They provide trend results for RO observations from 2002 to 2018 detecting a significant warming in the troposphere of $\sim 0.3 \text{ K decade}^{-1}$ (95% confidence level) and a cooling from -0.1 to $-0.2 \text{ K decade}^{-1}$ in the tropical lower stratosphere (Fig. 11).

Schmidt et al. (2008b, 2010b) and W. Wang et al. (2013) performed early studies on tropopause height and temperature trends. Due to significant natural variability, tropopause trends were inconclusive for short periods (Rieckh et al. 2014). A widening of the tropical belt deduced from RO tropopause statistics was found in the Northern Hemisphere from 2002 to 2011 (Ao and Hajj 2013; Davis and Birner 2013; Gleisner et al. 2015).

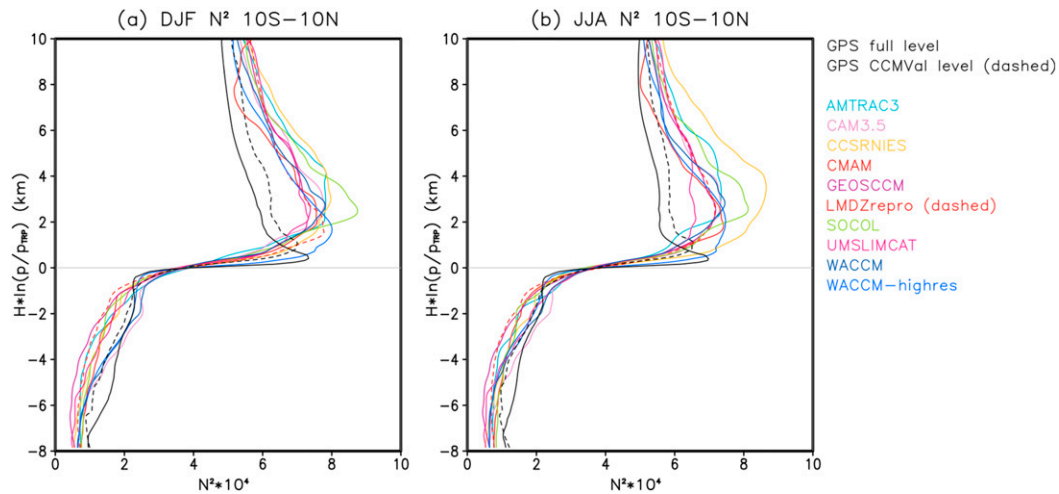


FIG. 12. Vertical profiles of the tropical tropopause inversion layer in terms of buoyancy frequency from CCMs and RO observations from April 2006 to April 2009 are shown for (a) DJF and (b) JJA. The profiles are organized with respect to the cold-point tropopause (Gettelman et al. 2010).

Short-term trends of RO observations have been compared with different satellite observations such as those from the Advanced Microwave Sounding Unit (AMSU) (Gleisner et al. 2015) and the Advanced Infrared Sounder (AIRS) (Leroy et al. 2018) as well as reanalyses (Shangguan et al. 2019). Khaykin et al. (2017) showed good agreement in lower stratospheric temperature trends between RO and *Aqua* AMSU records. A comparison of trends from RO observations and those from reanalyses assimilating various satellite observations, however, revealed significant biases in the reanalyses due to inherent discontinuities in assimilated observations and methods (Shangguan et al. 2019).

c. Climate model evaluation

Leroy and North (2000) investigated the application of RO for climate model evaluation. They showed that climate signal detection can be a useful method to test whether climate models reproduce trends and anomalies as revealed by the observations. Leroy et al. (2006a) tested future projections and climate change fingerprints in models from phase 3 of the Coupled Model Intercomparison Project (CMIP3), based on simulated RO pressure trends.

Ao et al. (2015) reported good agreement between models from phase 5 of CMIP (CMIP5) and RO observations in terms of the annual cycle and interannual variability of the tropical geopotential height at 200 hPa. In the extratropics, the agreement became poor with the largest model biases in high latitudes. By comparing UTLS temperature fields at selected pressure levels with COSMIC observations from 2006 to 2013, Kishore et al. (2016) concluded that the CMIP5 models reproduce the overall annual and interannual temperature variations, but have a large bias of about 2 K at 100 hPa on average.

Data from RO can be used for more detailed assessments of atmospheric climate models, such as on the effect of different model resolutions (e.g., Schmidt et al. 2016b). Steiner et al. (2018) investigated the representation of tropical convection in

the CMIP5 atmosphere-only models (AMIP), which are available at higher vertical resolution. They focused on the vertical structure in moist and dry regimes. Results showed that the tropical tropopause is poorly captured in most atmosphere models, with model temperature biases larger than 4 K in the tropopause region and the lower stratosphere. Results also revealed that some models do not fully capture the thermodynamic structure in regions of enhanced convection. In moist convection regions, models tend to underestimate moisture over the oceans, whereas in dry downdraft regions, they overestimate moisture up to 100%. These shortcomings of models were also discussed by Kursinski and Gebhardt (2014).

The RO observations were also used to evaluate the width of the tropical belt based on the tropopause and subtropical jet core metrics, showing that models tend to overestimate the mean width and underestimate its seasonal cycle amplitude (Davis and Birner 2016).

In the multimodel assessments of coupled chemistry–climate models (CCMs) by Gettelman et al. (2010) for the tropics and by Hegglin et al. (2010) for the extratropics, RO observations were used to evaluate the representation of the tropical and extratropical tropopause transition layers. The findings showed that a tropopause inversion layer is present in most models, but it is much weaker and thicker than observed in RO data, even when the observations are regridded to model levels (Fig. 12). Gettelman et al. (2010) explain the limited representation of the tropopause inversion layer and buoyancy frequency by coarse vertical model resolution and less adiabatic cooling associated with weak upwelling in the models.

9. Summary, conclusions, and outlook

GNSS radio occultation observations provide unique information on the thermal structure and variability of the tropical UTLS because of their high accuracy (low biases/systematic errors) and precision (low uncertainty) as well as high vertical

resolution, global availability, and long-term stability. The UTLS region is fundamental to many aspects of the climate system, showing strong spatial and temporal variability ranging from subseasonal to interannual time scales. RO data have been instrumental in quantifying these sources of variability due to their quasi-homogeneous coverage in time and space throughout the tropics.

Subseasonal variability associated with perturbations from gravity waves, atmospheric Kelvin waves, Rossby and mixed Rossby–gravity waves is well resolved by RO data. Even small-amplitude atmospheric thermal tides can be investigated due to complete local-time sampling at low latitudes. Insensitive to clouds and precipitation, RO observations reveal novel details of the structure of deep convection, tropical cyclones, and volcanic clouds. Data have also been exploited to study the UTLS response of the MJO, ENSO, and the QBO. Long-term stability and consistency make the almost two-decade-long RO record well suited to evaluate climate models and to study climate change.

Highlights of added value of RO for improving knowledge on tropical UTLS characteristics and behavior include the following:

- characterization of spatial and temporal variability of the tropical tropopause region;
- quantification of spatial and temporal characteristics of the tropopause inversion layer;
- detection of sharp vertical gradients associated with deep convection and tropical cyclones including cooling at the cloud top and development of secondary tropopauses;
- investigation of the modification of the atmospheric thermal structure due to volcanic clouds;
- quantification of GW vertical wavelengths, horizontal wavelengths, and momentum fluxes;
- characterization of equatorially trapped waves and their seasonal and interannual variability;
- characterization of subseasonal variability associated with the MJO;
- characterization of the three-dimensional thermal structure during ENSO events;
- quantification of vertically resolved short-term trends of different atmospheric parameters; and
- evaluation of other observational datasets, atmospheric analyses and reanalyses, and weather and climate models.

With the successful launch of COSMIC-2 in July 2019, the proliferation of commercial LEO satellites, and the use of more GNSS satellites besides GPS such as the Russian GLONASS or the European Galileo system, tropical sampling density will further increase, opening new potential to study fine-scale structures of the tropical UTLS. This will yield new insights on the morphology of the tropical UTLS and improve understanding of the atmospheric climate system.

Acknowledgments. We thank all RO processing teams worldwide for their continuous support and for making RO data available for free. At WEGC this work was funded by the Austrian Science Fund (FWF) under Research Grant P27724-NBL (VERTICLIM). The UCAR work was sponsored by

NSF-NASA Grant 1522830, NOAA Contract 16CN0070, U.S. Air Force Contract 319C004, and NSPO-UCAR AIT-TECRO Agreement Implementing Arrangement 5. Author Randel was additionally supported by the NASA GNSS Remote Sensing Science Team under Grant NNX16AK37G. Author Tsuda was supported in part by JSPS KAKENHI Grant JP18K03741. Author M. J. Alexander was supported by NASA Grant 80NSSC18K0069 and NSF Grant 1642644. Author Biondi was supported by the VESUVIO project funded under the Supporting Talent in Research (STARS) Programme at Università degli Studi di Padova, and by the H2020 SESAR ENGAGE KTN CARGO project under Grant Agreement 783287. Author Kim was supported by the National Research Foundation of Korea (NRF-2020R1F1A1075859). Author Son was supported by the National Research Foundation of Korea (NRF) grant funded by the South Korean government (Ministry of Science and ICT) (2017R1E1A1A01074889). The National Center for Atmospheric Research is sponsored by the U.S. National Science Foundation.

REFERENCES

- Alexander, M. J., 1996: A simulated spectrum of convectively generated gravity waves: Propagation from the tropopause to the mesopause and effects on the middle atmosphere. *J. Geophys. Res.*, **101**, 1571–1588, <https://doi.org/10.1029/95JD02046>.
- , 2015: Global and seasonal variations in three-dimensional gravity wave momentum flux from satellite limb-sounding temperatures. *Geophys. Res. Lett.*, **42**, 6860–6867, <https://doi.org/10.1002/2015GL065234>.
- , and D. A. Ortland, 2010: Equatorial waves in High Resolution Dynamics Limb Sounder (HIRDLs) data. *J. Geophys. Res.*, **115**, D24111, <https://doi.org/10.1029/2010JD014782>.
- Alexander, S. P., T. Tsuda, and Y. Kawatani, 2008a: COSMIC GPS observations of Northern Hemisphere winter stratospheric gravity waves and comparisons with an atmospheric general circulation model. *Geophys. Res. Lett.*, **35**, L10808, <https://doi.org/10.1029/2008GL033174>.
- , —, and M. Takahashi, 2008b: Global distribution of atmospheric waves in the equatorial upper troposphere and lower stratosphere: COSMIC observations of wave mean flow interactions. *J. Geophys. Res.*, **113**, D24115, <https://doi.org/10.1029/2008JD010039>.
- , A. R. Klekociuk, A. J. McDonald, and M. C. Pitts, 2013: Quantifying the role of orographic gravity waves on polar stratospheric cloud occurrence in the Antarctic and the Arctic. *J. Geophys. Res. Atmos.*, **118**, 11 493–11 507, <https://doi.org/10.1002/2013JD020122>.
- Angerer, B., F. Ladstädter, B. Scherllin-Pirscher, M. Schwärz, A. K. Steiner, U. Foelsche, and G. Kirchengast, 2017: Quality aspects of the Wegener Center multi-satellite GPS radio occultation record OPSv5.6. *Atmos. Meas. Tech.*, **10**, 4845–4863, <https://doi.org/10.5194/amt-10-4845-2017>.
- Anthes, R. A., and W. S. Schreiner, 2019: Six new satellites watch the atmosphere over Earth's equator. *Eos*, **100**, <https://doi.org/10.1029/2019EO131779>.
- , C. Rocken, and Y.-H. Kuo, 2000: Applications of COSMIC to meteorology and climate. *Terr. Atmos. Ocean. Sci.*, **11**, 115–156, [https://doi.org/10.3319/TAO.2000.11.1.115\(COSMIC\)](https://doi.org/10.3319/TAO.2000.11.1.115(COSMIC)).
- , and Coauthors, 2008: The COSMIC/FORMOSAT-3 mission: Early results. *Bull. Amer. Meteor. Soc.*, **89**, 313–334, <https://doi.org/10.1175/BAMS-89-3-313>.

- Ao, C. O., and A. J. Hajj, 2013: Monitoring the width of the tropical belt with GPS radio occultation measurements. *Geophys. Res. Lett.*, **40**, 6236–6241, <https://doi.org/10.1002/2013GL058203>.
- , W. S. Schreiner, and J. Wickert, 2003: First report on the CHAMP radio occultation intercomparison study. JPL Publ. 03-016.
- , G. A. Hajj, B. A. Iijima, A. J. Mannucci, T. M. Schröder, M. de la Torre Juárez, and S. S. Leroy, 2006: Sensitivity of stratospheric retrievals from radio occultations on upper boundary conditions. *Atmosphere and Climate: Studies by Occultation Methods*, U. Foelsche, G. Kirchengast, and A. K. Steiner, Eds., Springer, 17–26.
- , A. J. Mannucci, and E. R. Kursinski, 2012: Improving GPS radio occultation stratospheric refractivity retrievals for climate benchmarking. *Geophys. Res. Lett.*, **39**, L12701, <https://doi.org/10.1029/2012GL051720>.
- , and Coauthors, 2015: Evaluation of CMIP5 upper troposphere and lower stratosphere geopotential height with GPS radio occultation observations. *J. Geophys. Res. Atmos.*, **120**, 1678–1689, <https://doi.org/10.1002/2014JD022239>.
- Baldwin, M. P., and Coauthors, 2001: The quasi-biennial oscillation. *Rev. Geophys.*, **39**, 179–229, <https://doi.org/10.1029/1999RG000073>.
- Bell, S. W., and M. A. Geller, 2008: Tropopause inversion layer: Seasonal and latitudinal variations and representation in standard radiosonde data and global models. *J. Geophys. Res.*, **113**, D05109, <https://doi.org/10.1029/2007JD009022>.
- Biondi, R., T. Neubert, S. Syndergaard, and J. K. Nielsen, 2011a: Measurements of the upper troposphere and lower stratosphere during tropical cyclones using the GPS radio occultation technique. *Adv. Space Res.*, **47**, 348–355, <https://doi.org/10.1016/j.asr.2010.05.031>.
- , —, —, and —, 2011b: Radio occultation bending angle anomalies during tropical cyclones. *Atmos. Meas. Tech.*, **4**, 1053–1060, <https://doi.org/10.5194/amt-4-1053-2011>.
- , W. J. Randel, S.-P. Ho, T. Neubert, and S. Syndergaard, 2012: Thermal structure of intense convective clouds derived from GPS radio occultations. *Atmos. Chem. Phys.*, **12**, 5309–5318, <https://doi.org/10.5194/acp-12-5309-2012>.
- , S.-P. Ho, W. J. Randel, S. Syndergaard, and T. Neubert, 2013: Tropical cyclone cloud-top height and vertical temperature structure detection using GPS radio occultation measurements. *J. Geophys. Res. Atmos.*, **118**, 5247–5259, <https://doi.org/10.1002/jgrd.50448>.
- , A. K. Steiner, G. Kirchengast, and T. Rieckh, 2015: Characterization of thermal structure and conditions for overshooting of tropical and extratropical cyclones with GPS radio occultation. *Atmos. Chem. Phys.*, **15**, 5181–5193, <https://doi.org/10.5194/acp-15-5181-2015>.
- , —, —, H. Brenot, and T. Rieckh, 2017: Supporting the detection and monitoring of volcanic clouds: A promising new application of Global Navigation Satellite System radio occultation. *Adv. Space Res.*, **60**, 2707–2722, <https://doi.org/10.1016/j.asr.2017.06.039>.
- Birner, T., and E. J. Charlesworth, 2017: On the relative importance of radiative and dynamical heating for tropical tropopause temperatures. *J. Geophys. Res. Atmos.*, **122**, 6782–6797, <https://doi.org/10.1002/2016JD026445>.
- , D. Sankey, and T. G. Shepherd, 2006: The tropopause inversion layer in models and analyses. *Geophys. Res. Lett.*, **33**, L14804, <https://doi.org/10.1029/2006GL026549>.
- Bojinski, S., M. Verstraete, T. C. Peterson, C. Richter, A. Simmons, and M. Zemp, 2014: The concept of essential climate variables in support of climate research, applications, and policy. *Bull. Amer. Meteor. Soc.*, **95**, 1431–1443, <https://doi.org/10.1175/BAMS-D-13-00047.1>.
- Bonafoni, S., and R. Biondi, 2016: The usefulness of the Global Navigation Satellite Systems (GNSS) in the analysis of precipitation events. *Atmos. Res.*, **167**, 15–23, <https://doi.org/10.1016/j.atmosres.2015.07.011>.
- , —, H. Brenot, and R. Anthes, 2019: Radio occultation and ground-based GNSS products for observing, understanding and predicting extreme events: A review. *Atmos. Res.*, **230**, 104624, <https://doi.org/10.1016/j.atmosres.2019.104624>.
- Borsche, M., G. Kirchengast, and U. Foelsche, 2007: Tropical tropopause climatology as observed with radio occultation measurements from CHAMP compared to ECMWF and NCEP analyses. *Geophys. Res. Lett.*, **34**, L03702, <https://doi.org/10.1029/2006GL027918>.
- Brewer, M. A., 1949: Evidence for a world circulation provided by measurements of helium and water vapor distribution in the stratosphere. *Quart. J. Roy. Meteor. Soc.*, **75**, 351–363, <https://doi.org/10.1002/qj.49707532603>.
- Calvo Fernández, N., R. R. García, R. G. Herrera, D. G. Puyol, L. G. Presa, E. H. Martín, and P. R. Rodríguez, 2004: Analysis of the ENSO signal in tropospheric and stratospheric temperatures observed by MSU, 1979–2000. *J. Climate*, **17**, 3934–3946, [https://doi.org/10.1175/1520-0442\(2004\)017<3934:AOTESI>2.0.CO;2](https://doi.org/10.1175/1520-0442(2004)017<3934:AOTESI>2.0.CO;2).
- Chane Ming, F., C. Ibrahim, C. Barthe, S. Jolivet, P. Keckhut, Y.-A. Liou, and Y. Kuleshov, 2014: Observation and a numerical study of gravity waves during Tropical Cyclone Ivan (2008). *Atmos. Chem. Phys.*, **14**, 641–658, <https://doi.org/10.5194/acp-14-641-2014>.
- Cigala, V., R. Biondi, A. J. Prata, A. K. Steiner, G. Kirchengast, and H. Brenot, 2019: GNSS radio occultation advances the monitoring of volcanic clouds: The case of the 2008 Kasatochi eruption. *Remote Sens.*, **11**, 2199, <https://doi.org/10.3390/rs11192199>.
- Danzer, J., B. Scherllin-Pirscher, and U. Foelsche, 2013: Systematic residual ionospheric errors in radio occultation data and a potential way to minimize them. *Atmos. Meas. Tech.*, **6**, 2169–2179, <https://doi.org/10.5194/amt-6-2169-2013>.
- , U. Foelsche, B. Scherllin-Pirscher, and M. Schwarz, 2014a: Influence of changes in humidity on dry temperature in GPS RO climatologies. *Atmos. Meas. Tech.*, **7**, 2883–2896, <https://doi.org/10.5194/amt-7-2883-2014>.
- , H. Gleisner, and S. B. Healy, 2014b: CHAMP climate data based on the inversion of monthly average bending angles. *Atmos. Meas. Tech.*, **7**, 4071–4079, <https://doi.org/10.5194/amt-7-4071-2014>.
- , S. B. Healy, and I. D. Culverwell, 2015: A simulation study with a new residual ionospheric error model for GPS radio occultation climatologies. *Atmos. Meas. Tech.*, **8**, 3395–3404, <https://doi.org/10.5194/amt-8-3395-2015>.
- , M. Schwarz, V. Proschek, U. Foelsche, and H. Gleisner, 2018: Comparison study of COSMIC RO dry-air climatologies based on average profile inversion. *Atmos. Meas. Tech.*, **11**, 4867–4882, <https://doi.org/10.5194/amt-11-4867-2018>.
- Davis, N., and T. Birner, 2016: Climate model biases in the width of the tropical belt. *J. Climate*, **29**, 1935–1954, <https://doi.org/10.1175/JCLI-D-15-0336.1>.
- Davis, N. A., and T. Birner, 2013: Seasonal to multidecadal variability of the width of the tropical belt. *J. Geophys. Res. Atmos.*, **118**, 7773–7787, <https://doi.org/10.1002/jgrd.50610>.

- de la Torre, A., T. Tsuda, G. A. Hajj, and J. Wickert, 2004: A global distribution of the stratospheric gravity wave activity from GPS occultation profiles with *SAC-C* and *CHAMP*. *J. Meteor. Soc. Japan*, **82**, 407–417, <https://doi.org/10.2151/jmsj.2004.407>.
- , T. Schmidt, and J. Wickert, 2006: A global analysis of wave potential energy in the lower stratosphere derived from 5 years of GPS radio occultation data with *CHAMP*. *Geophys. Res. Lett.*, **33**, L24809, <https://doi.org/10.1029/2006GL027696>.
- , P. Llamedo, P. Alexander, T. Schmidt, and J. Wickert, 2010: Estimated errors in a global gravity wave climatology from GPS radio occultation temperature profiles. *Adv. Space Res.*, **46**, 174–179, <https://doi.org/10.1016/j.asr.2010.02.033>.
- , P. Alexander, T. Schmidt, P. Llamedo, and R. Hierro, 2018: On the distortions in calculated GW parameters during slanted atmospheric soundings. *Atmos. Meas. Tech.*, **11**, 1363–1375, <https://doi.org/10.5194/amt-11-1363-2018>.
- Dima, I. M., and J. M. Wallace, 2007: Structure of the annual-mean equatorial planetary waves in the ERA-40 reanalyses. *J. Atmos. Sci.*, **64**, 2862–2880, <https://doi.org/10.1175/JAS3985.1>.
- Ern, M., P. Preusse, M. J. Alexander, and C. D. Warner, 2004: Absolute values of gravity wave momentum flux derived from satellite data. *J. Geophys. Res.*, **109**, D20103, <https://doi.org/10.1029/2004JD004752>.
- , —, M. Krebsbach, M. G. Mlynzack, and J. M. Russell III, 2008: Equatorial wave analysis from SABER and ECMWF temperatures. *Atmos. Chem. Phys.*, **8**, 845–869, <https://doi.org/10.5194/acp-8-845-2008>.
- Faber, A., P. Llamedo, T. Schmidt, A. de la Torre, and J. Wickert, 2013: On the determination of gravity wave momentum flux from GPS radio occultation data. *Atmos. Meas. Tech.*, **6**, 3169–3180, <https://doi.org/10.5194/amt-6-3169-2013>.
- Feltz, M. L., R. O. Knuteson, H. E. Revercomb, and D. C. Tobin, 2014: A methodology for the validation of temperature profiles from hyperspectral infrared sounders using GPS radio occultation: Experience with AIRS and COSMIC. *J. Geophys. Res. Atmos.*, **119**, 1680–1691, <https://doi.org/10.1002/2013JD020853>.
- Feng, D. D., and B. M. Herman, 1999: Remotely sensing the Earth's atmosphere using the global positioning system (GPS)—The GPS/MET data analysis. *J. Atmos. Oceanic Technol.*, **16**, 989–1002, [https://doi.org/10.1175/1520-0426\(1999\)016<0989:RSTESA>2.0.CO;2](https://doi.org/10.1175/1520-0426(1999)016<0989:RSTESA>2.0.CO;2).
- Flannaghan, T. J., and S. Fueglistaler, 2013: The importance of the tropical tropopause layer for equatorial Kelvin wave propagation. *J. Geophys. Res. Atmos.*, **118**, 5160–5175, <https://doi.org/10.1002/jgrd.50418>.
- Foelsche, U., M. Borsche, A. K. Steiner, A. Gobiet, B. Pirscher, G. Kirchengast, J. Wickert, and T. Schmidt, 2008a: Observing upper troposphere-lower stratosphere climate with radio occultation data from the *CHAMP* satellite. *Climate Dyn.*, **31**, 49–65, <https://doi.org/10.1007/s00382-007-0337-7>.
- , G. Kirchengast, A. K. Steiner, L. Kornblueh, E. Manzini, and L. Bengtsson, 2008b: An observing system simulation experiment for climate monitoring with GNSS radio occultation data: Setup and test bed study. *J. Geophys. Res.*, **113**, D11108, <https://doi.org/10.1029/2007JD009231>.
- , B. Scherllin-Pirscher, F. Ladstädter, A. K. Steiner, and G. Kirchengast, 2011a: Refractivity and temperature climate records from multiple radio occultation satellites consistent within 0.05%. *Atmos. Meas. Tech.*, **4**, 2007–2018, <https://doi.org/10.5194/amt-4-2007-2011>.
- , S. Syndergaard, J. Fritzer, and G. Kirchengast, 2011b: Errors in GNSS radio occultation data: Relevance of the measurement geometry and obliquity of profiles. *Atmos. Meas. Tech.*, **4**, 189–199, <https://doi.org/10.5194/amt-4-189-2011>.
- Fueglistaler, S., A. E. Dessler, T. J. Dunkerton, I. Folkins, Q. Fu, and P. W. Mote, 2009: Tropical tropopause layer. *Rev. Geophys.*, **47**, RG1004, <https://doi.org/10.1029/2008RG000267>.
- , P. H. Haynes, and P. M. Forster, 2011: The annual cycle in lower stratospheric temperatures revisited. *Atmos. Chem. Phys.*, **11**, 3701–3711, <https://doi.org/10.5194/acp-11-3701-2011>.
- Fujiwara, M., and Coauthors, 2017: Introduction to the SPARC Reanalysis Intercomparison Project (S-RIP) and overview of the reanalysis systems. *Atmos. Chem. Phys.*, **17**, 1417–1452, <https://doi.org/10.5194/acp-17-1417-2017>.
- Garcia, R. R., and M. L. Salby, 1987: Transient response to localized episodic heating in the tropics. Part II: Far-field behavior. *J. Atmos. Sci.*, **44**, 499–532, [https://doi.org/10.1175/1520-0469\(1987\)044<0499:TRTLEH>2.0.CO;2](https://doi.org/10.1175/1520-0469(1987)044<0499:TRTLEH>2.0.CO;2).
- GCOS, 2011: Systematic observation requirements for satellite-based products for climate (2011 update). Global Climate Observing System Doc. GCOS-154, 138 pp., https://library.wmo.int/doc_num.php?explnum_id=3710.
- , 2016: The global observing system for climate: Implementation needs. Global Climate Observing System Doc. GCOS-200, 341 pp., https://library.wmo.int/doc_num.php?explnum_id=3417.
- Geller, M. A., and Coauthors, 2013: A comparison between gravity wave momentum fluxes in observations and climate models. *J. Climate*, **26**, 6383–6405, <https://doi.org/10.1175/JCLI-D-12-00545.1>.
- Gettelman, A., and Coauthors, 2010: Multimodel assessment of the upper troposphere and lower stratosphere: Tropics and global trends. *J. Geophys. Res.*, **115**, D00M08, <https://doi.org/10.1029/2009JD013638>.
- Gill, A. E., 1980: Some simple solutions for heat-induced tropical circulation. *Quart. J. Roy. Meteor. Soc.*, **106**, 447–462, <https://doi.org/10.1002/qj.49710644905>.
- Gilpin, S., T. Rieckh, and R. Anthes, 2018: Reducing representativeness and sampling errors in radio occultation–radiosonde comparisons. *Atmos. Meas. Tech.*, **11**, 2567–2582, <https://doi.org/10.5194/amt-11-2567-2018>.
- Gleisner, H., and S. B. Healy, 2013: A simplified approach for generating GNSS radio occultation refractivity climatologies. *Atmos. Meas. Tech.*, **6**, 121–129, <https://doi.org/10.5194/amt-6-121-2013>.
- , P. Thejll, B. Christiansen, and J. K. Nielsen, 2015: Recent global warming hiatus dominated by low-latitude temperature trends in surface and troposphere data. *Geophys. Res. Lett.*, **42**, 510–517, <https://doi.org/10.1002/2014GL062596>.
- Gobiet, A., G. Kirchengast, G. L. Manney, M. Borsche, C. Retscher, and G. Stiller, 2007: Retrieval of temperature profiles from *CHAMP* for climate monitoring: Intercomparison with Envisat MIPAS and GOMOS and different atmospheric analyses. *Atmos. Chem. Phys.*, **7**, 3519–3536, <https://doi.org/10.5194/acp-7-3519-2007>.
- Goody, R., J. Anderson, and G. North, 1998: Testing climate models: An approach. *Bull. Amer. Meteor. Soc.*, **79**, 2541–2549, [https://doi.org/10.1175/1520-0477\(1998\)079<2541:TCMAA>2.0.CO;2](https://doi.org/10.1175/1520-0477(1998)079<2541:TCMAA>2.0.CO;2).
- , —, T. Karl, R. B. Miller, G. North, J. Simpson, G. Stephens, and W. Washington, 2002: Why we should monitor the climate. *Bull. Amer. Meteor. Soc.*, **83**, 873–878, [https://doi.org/10.1175/1520-0477\(2002\)083<0873:WWSMTC>2.3.CO;2](https://doi.org/10.1175/1520-0477(2002)083<0873:WWSMTC>2.3.CO;2).
- Grise, K. M., D. W. J. Thompson, and T. Birner, 2010: A global survey of static stability in the stratosphere and upper troposphere. *J. Climate*, **23**, 2275–2292, <https://doi.org/10.1175/2009JCLI3369.1>.

- Haase, J. S., and Coauthors, 2018: Around the world in 84 days. *Eos, Trans. Amer. Geophys. Union*, **99**, <https://doi.org/10.1029/2018EO091907>.
- Hagan, M. E., and J. M. Forbes, 2002: Migrating and nonmigrating diurnal tides in the middle and upper atmosphere excited by tropospheric latent heat release. *J. Geophys. Res.*, **107**, 4754, <https://doi.org/10.1029/2001JD001236>.
- , and —, 2003: Migrating and nonmigrating semidiurnal tides in the upper atmosphere excited by tropospheric latent heat release. *J. Geophys. Res.*, **108**, 1062, <https://doi.org/10.1029/2002JA009466>.
- Hajj, G. A., E. R. Kursinski, L. J. Romans, W. I. Bertiger, and S. S. Leroy, 2002: A technical description of atmospheric sounding by GPS occultation. *J. Atmos. Sol.-Terr. Phys.*, **64**, 451–469, [https://doi.org/10.1016/S1364-6826\(01\)00114-6](https://doi.org/10.1016/S1364-6826(01)00114-6).
- , and Coauthors, 2004: CHAMP and SAC-C atmospheric occultation results and intercomparisons. *J. Geophys. Res.*, **109**, D06109, <https://doi.org/10.1029/2003JD003909>.
- He, W., S.-P. Ho, H. Chen, X. Zhou, D. Hunt, and Y.-H. Kuo, 2009: Assessment of radiosonde temperature measurements in the upper troposphere and lower stratosphere using COSMIC radio occultation data. *Geophys. Res. Lett.*, **36**, L17807, <https://doi.org/10.1029/2009GL038712>.
- Healy, S. B., and I. D. Culverwell, 2015: A modification to the standard ionospheric correction method used in GPS radio occultation. *Atmos. Meas. Tech.*, **8**, 3385–3393, <https://doi.org/10.5194/amt-8-3385-2015>.
- , I. Polichtchouk, and A. Horanyi, 2020: Zonal wind information in the tropical stratosphere provided by GNSS radio occultation. *Quart. J. Roy. Meteor. Soc.*, **146**, 3612–3621, <https://doi.org/10.1002/qj.3870>.
- Hegglin, M. I., and Coauthors, 2010: Multimodel assessment of the upper troposphere and lower stratosphere: Extratropics. *J. Geophys. Res.*, **115**, D00M09, <https://doi.org/10.1029/2010JD013884>.
- Hendon, H. H., and S. Abhik, 2018: Differences in vertical structure of the Madden-Julian oscillation associated with the quasi-biennial oscillation. *Geophys. Res. Lett.*, **45**, 4419–4428, <https://doi.org/10.1029/2018GL077207>.
- Hersbach, H., and Coauthors, 2020: The ERA5 global reanalysis. *Quart. J. Roy. Meteor. Soc.*, **146**, 1999–2049, <https://doi.org/10.1002/qj.3803>.
- Ho, S.-P., Y.-H. Kuo, Z. Zeng, and T. Peterson, 2007: A comparison of lower stratospheric temperature from microwave measurements with CHAMP GPS RO data. *Geophys. Res. Lett.*, **34**, L15701, <https://doi.org/10.1029/2007GL030202>.
- , and Coauthors, 2009: Estimating the uncertainty of using GPS radio occultation data for climate monitoring: Intercomparison of CHAMP refractivity climate records from 2002 to 2006 from different data centers. *J. Geophys. Res.*, **114**, D23107, <https://doi.org/10.1029/2009JD011969>.
- , and Coauthors, 2012: Reproducibility of GPS radio occultation data for climate monitoring: Profile-to-profile intercomparison of CHAMP climate records 2002 to 2008 from six data centers. *J. Geophys. Res.*, **117**, D18111, <https://doi.org/10.1029/2012JD017665>.
- , and Coauthors, 2020: The COSMIC/FORMOSAT-3 radio occultation mission after 12 years: Accomplishments, remaining challenges, and potential impacts of COSMIC-2. *Bull. Amer. Meteor. Soc.*, **101**, E1107–E1136, <https://doi.org/10.1175/BAMS-D-18-0290.1>.
- Hocke, K., 1997: Inversion of GPS meteorology data. *Ann. Geophys.*, **15**, 443–450, <https://doi.org/10.1007/s00585-997-0443-1>.
- Holton, J. R., M. J. Alexander, and M. T. Boehm, 2001: Evidence for short vertical wavelength Kelvin waves in the Department of Energy–Atmospheric Radiation Measurement Nauru99 radiosonde data. *J. Geophys. Res.*, **106**, 20 125–20 129, <https://doi.org/10.1029/2001JD900108>.
- Horinouchi, T., and T. Tsuda, 2009: Spatial structures and statistics of atmospheric gravity waves derived using a heuristic vertical cross-section extraction from COSMIC GPS radio occultation data. *J. Geophys. Res.*, **114**, D16110, <https://doi.org/10.1029/2008JD011068>.
- Jensen, E., and L. Pfister, 2004: Transport and freeze-drying in the tropical tropopause layer. *J. Geophys. Res.*, **109**, D02207, <https://doi.org/10.1029/2003JD004022>.
- Jin, S., G. P. Feng, and S. Gleason, 2011: Remote sensing using GNSS signals: Current status and future directions. *Adv. Space Res.*, **47**, 1645–1653, <https://doi.org/10.1016/j.asr.2011.01.036>.
- Johnston, B. R., F. Xie, and C. Liu, 2018: The effects of deep convection on regional temperature structure in the tropical upper troposphere and lower stratosphere. *J. Geophys. Res. Atmos.*, **123**, 1585–1603, <https://doi.org/10.1002/2017JD027120>.
- Kawatani, Y., S. K. Dhaka, M. Takahashi, and T. Tsuda, 2003: Large potential energy of gravity waves over a smooth surface with little convection: Simulation and observation. *Geophys. Res. Lett.*, **30**, 1438, <https://doi.org/10.1029/2003GL019690>.
- , M. Takahashi, K. Sato, S. P. Alexander, and T. Tsuda, 2009: Global distribution of atmospheric waves in the equatorial upper troposphere and lower stratosphere: AGCM simulation of sources and propagation. *J. Geophys. Res.*, **114**, D01102, <https://doi.org/10.1029/2008JD010374>.
- Khaykin, S. M., J.-P. Pommereau, and A. Hauchecorne, 2013: Impact of land convection on temperature diurnal variation in the tropical lower stratosphere inferred from COSMIC GPS radio occultations. *Atmos. Chem. Phys.*, **13**, 6391–6402, <https://doi.org/10.5194/acp-13-6391-2013>.
- , and Coauthors, 2017: Postmillennium changes in stratospheric temperature consistently resolved by GPS radio occultation and AMSU observations. *Geophys. Res. Lett.*, **44**, 7510–7518, <https://doi.org/10.1002/2017GL074353>.
- Kiladis, G. N., K. H. Straub, G. C. Reid, and K. S. Gage, 2001: Aspects of interannual and intraseasonal variability of the tropopause and lower stratosphere. *Quart. J. Roy. Meteor. Soc.*, **127**, 1961–1983, <https://doi.org/10.1002/qj.49712757606>.
- Kim, J., and S.-W. Son, 2012: Tropical cold-point tropopause: Climatology, seasonal cycle, and intraseasonal variability derived from COSMIC GPS radio occultation measurements. *J. Climate*, **25**, 5343–5360, <https://doi.org/10.1175/JCLI-D-11-00554.1>.
- , K. M. Grise, and S.-W. Son, 2013: Thermal characteristics of the cold-point tropopause region in CMIP5 models. *J. Geophys. Res. Atmos.*, **118**, 8827–8841, <https://doi.org/10.1002/jgrd.50649>.
- , W. J. Randel, T. Birner, and M. Abalos, 2016: Spectrum of wave forcing associated with the annual cycle of upwelling at the tropical tropopause. *J. Atmos. Sci.*, **73**, 855–868, <https://doi.org/10.1175/JAS-D-15-0096.1>.
- , —, and —, 2018: Convectively driven tropopause-level cooling and its influences on stratosphere moisture. *J. Geophys. Res. Atmos.*, **123**, 590–606, <https://doi.org/10.1002/2017JD027080>.
- Kim, J.-E., and M. J. Alexander, 2015: Direct impacts of waves on tropical cold point tropopause temperature. *Geophys. Res. Lett.*, **42**, 1584–1592, <https://doi.org/10.1002/2014GL062737>.

- , and Coauthors, 2016: Ubiquitous influence of waves on tropical high cirrus clouds. *Geophys. Res. Lett.*, **43**, 5895–5901, <https://doi.org/10.1002/2016GL069293>.
- Kishore, P., G. Basha, M. Venkat Ratnam, I. Velicogna, T. B. M. J. Ouarda, and D. Narayana Rao, 2016: Evaluating CMIP5 models using GPS radio occultation COSMIC temperature in UTLS region during 2006–2013: Twenty-first century projection and trends. *Climate Dyn.*, **47**, 3253–3270, <https://doi.org/10.1007/s00382-016-3024-8>.
- Kumar, V., S. K. Dhaka, R. K. Choudhary, S.-P. Ho, S. Yoden, and K. K. Reddy, 2014: On the occurrence of the coldest region in the stratosphere and tropical tropopause stability: A study using COSMIC/FORMOSAT-3 satellite measurements. *J. Atmos. Sol.-Terr. Phys.*, **121**, 271–286, <https://doi.org/10.1016/j.jastp.2014.10.007>.
- Kuo, Y.-H., T.-K. Wee, S. Sokolovskiy, C. Rocken, W. Schreiner, D. Hunt, and R. A. Anthes, 2004: Inversion and error estimation of GPS radio occultation data. *J. Meteor. Soc. Japan*, **82**, 507–531, <https://doi.org/10.2151/jmsj.2004.507>.
- , W. S. Schreiner, J. Wang, D. L. Rossiter, and Y. Zhang, 2005: Comparison of GPS radio occultation soundings with radiosondes. *Geophys. Res. Lett.*, **32**, L05817, <https://doi.org/10.1029/2004GL021443>.
- Kursinski, E. R., and T. Gebhardt, 2014: A method to deconvolve errors in GPS RO-derived water vapor histograms. *J. Atmos. Oceanic Technol.*, **31**, 2606–2628, <https://doi.org/10.1175/JTECH-D-13-00233.1>.
- , G. A. Hajj, J. T. Schofield, R. P. Linfield, and K. R. Hardy, 1997: Observing Earth's atmosphere with radio occultation measurements using the global positioning system. *J. Geophys. Res.*, **102**, 23 429–23 465, <https://doi.org/10.1029/97JD01569>.
- Lackner, B. C., A. K. Steiner, and G. Kirchengast, 2011a: Where to see climate change best in radio occultation variables—Study using GCMs and ECMWF reanalyses. *Ann. Geophys.*, **29**, 2147–2167, <https://doi.org/10.5194/angeo-29-2147-2011>.
- , —, —, and G. C. Hegerl, 2011b: Atmospheric climate change detection by radio occultation data using a fingerprinting method. *J. Climate*, **24**, 5275–5291, <https://doi.org/10.1175/2011JCLI3966.1>.
- Ladstätter, F., A. K. Steiner, U. Foelsche, L. Haimberger, C. Tavolato, and G. Kirchengast, 2011: An assessment of differences in lower stratospheric temperature records from (A) MSU, radiosondes, and GPS radio occultation. *Atmos. Meas. Tech.*, **4**, 1965–1977, <https://doi.org/10.5194/amt-4-1965-2011>.
- , —, M. Schwarz, and G. Kirchengast, 2015: Climate inter-comparison of GPS radio occultation, RS90/92 radiosondes and GRUAN from 2002 to 2013. *Atmos. Meas. Tech.*, **8**, 1819–1834, <https://doi.org/10.5194/amt-8-1819-2015>.
- Lasota, E., A. K. Steiner, G. Kirchengast, and R. Biondi, 2020: Tropical cyclones vertical structure from GNSS radio occultation: An archive covering the period 2001–2018. *Earth Syst. Sci. Data*, **12**, 2679–2693, <https://doi.org/10.5194/essd-12-2679-2020>.
- Leroy, S. S., 1997: Measurements of geopotential heights by GPS radio occultation. *J. Geophys. Res.*, **102**, 6971–6986, <https://doi.org/10.1029/96JD03083>.
- , and G. R. North, 2000: The application of COSMIC data to global change research. *Terr. Atmos. Ocean. Sci.*, **11**, 187–210, [https://doi.org/10.3319/TAO.2000.11.1.187\(COSMIC\)](https://doi.org/10.3319/TAO.2000.11.1.187(COSMIC)).
- , J. G. Anderson, and J. A. Dykema, 2006a: Testing climate models using GPS radio occultation: A sensitivity analysis. *J. Geophys. Res.*, **111**, D17105, <https://doi.org/10.1029/2005JD006145>.
- , J. A. Dykema, and J. G. Anderson, 2006b: Climate benchmarking using GNSS occultation. *Atmosphere and Climate: Studies by Occultation Methods*, U. Foelsche, G. Kirchengast, and A. K. Steiner, Eds., Springer, 287–302.
- , C. Ao, and O. P. Verkhoglyadova, 2012: Mapping GPS radio occultation data by Bayesian interpolation. *J. Atmos. Oceanic Technol.*, **29**, 1062–1074, <https://doi.org/10.1175/JTECH-D-11-00179.1>.
- , —, and —, 2018: Temperature trends and anomalies in modern satellite data: Infrared sounding and GPS radio occultation. *J. Geophys. Res. Atmos.*, **123**, 11 431–11 444, <https://doi.org/10.1029/2018JD028990>.
- Lewis, H. W., 2009: A robust method for tropopause altitude identification using GPS radio occultation data. *Geophys. Res. Lett.*, **36**, L12808, <https://doi.org/10.1029/2009GL039231>.
- Li, Y., G. Kirchengast, B. Scherllin-Pirscher, M. Schwarz, J. K. Nielsen, S.-P. Ho, and Y.-B. Yuan, 2019: A new algorithm for the retrieval of atmospheric profiles from GNSS radio occultation data in moist air and comparison to 1DVar retrievals. *Remote Sens.*, **11**, 2729, <https://doi.org/10.3390/rs11232729>.
- Lindzen, R. S., 1967: Planetary waves on beta-planes. *Mon. Wea. Rev.*, **95**, 441–451, [https://doi.org/10.1175/1520-0493\(1967\)095<0441:PWOBP>2.3.CO;2](https://doi.org/10.1175/1520-0493(1967)095<0441:PWOBP>2.3.CO;2).
- Löscher, A., K. B. Lauritsen, and M. Sørensen, 2009: The GRAS SAF radio occultation processing intercomparison project ROPIC. *New Horizons in Occultation Research: Studies in Atmosphere and Climate*, A. K. Steiner et al., Eds., Springer-Verlag, 49–62.
- Luna, D., P. Alexander, and A. de la Torre, 2013: Evaluation of uncertainty in gravity wave potential energy calculations through GPS radio occultation measurements. *Adv. Space Res.*, **52**, 879–882, <https://doi.org/10.1016/j.asr.2013.05.015>.
- Luntama, J.-P., and Coauthors, 2008: Prospects of the EPS GRAS mission for operational atmospheric applications. *Bull. Amer. Meteor. Soc.*, **89**, 1863–1876, <https://doi.org/10.1175/2008BAMS2399.1>.
- Matsuno, T., 1966: Quasi-geostrophic motions in the equatorial area. *J. Meteor. Soc. Japan*, **44**, 25–43, https://doi.org/10.2151/jmsj1965.44.1_25.
- McDonald, A. J., 2012: Gravity wave occurrence statistics derived from paired COSMIC/FORMOSAT3 observations. *J. Geophys. Res.*, **117**, D15106, <https://doi.org/10.1029/2011JD016715>.
- Mehta, S. K., M. V. Ratnam, and B. V. K. Murthy, 2011: Multiple tropopauses in the tropics: A cold point approach. *J. Geophys. Res.*, **116**, D20105, <https://doi.org/10.1029/2011JD016637>.
- , —, and —, 2013: Characteristics of the multiple tropopauses in the tropics. *J. Atmos. Sol.-Terr. Phys.*, **95–96**, 78–86, <https://doi.org/10.1016/j.jastp.2013.01.009>.
- , M. Fujiwara, T. Tsuda, and J.-P. Vernier, 2015: Effect of recent minor volcanic eruptions on temperatures in the upper troposphere and lower stratosphere. *J. Atmos. Sol.-Terr. Phys.*, **129**, 99–110, <https://doi.org/10.1016/j.jastp.2015.04.009>.
- Melbourne, W. G., and Coauthors, 1994: The application of spaceborne GPS to atmospheric limb sounding and global change monitoring. Jet Propulsion Laboratory Publ. 94-18, 147 pp., <https://ntrs.nasa.gov/citations/19960008694>.
- Ming, A., A. C. Maycock, P. Hitchcock, and P. Haynes, 2017: The radiative role of ozone and water vapour in the annual temperature cycle in the tropical tropopause layer. *Atmos. Chem. Phys.*, **17**, 5677–5701, <https://doi.org/10.5194/acp-17-5677-2017>.
- Mote, P. W., and Coauthors, 1996: An atmospheric tape recorder: The imprint of tropical tropopause temperatures on

- stratospheric water vapor. *J. Geophys. Res.*, **101**, 3989–4006, <https://doi.org/10.1029/95JD03422>.
- Munchak, L. A., and L. L. Pan, 2014: Separation of the lapse rate and the cold point tropopause in the tropics and the resulting impact on cloud top-tropopause relationships. *J. Geophys. Res. Atmos.*, **119**, 7963–7978, <https://doi.org/10.1002/2013JD021189>.
- Narayana Rao, D., M. V. Ratnam, B. V. K. Murthy, V. V. M. J. Rao, S. K. Mehta, D. Nath, and S. G. Basha, 2007: Identification of tropopause using bending angle profile from GPS radio occultation (RO): A radio tropopause. *Geophys. Res. Lett.*, **34**, L15809, <https://doi.org/10.1029/2007GL029709>.
- Nath, D., W. Chen, and A. Guharay, 2015: Climatology of stratospheric gravity waves and their interaction with zonal mean wind over the tropics using GPS RO and ground-based measurements in the two phases of QBO. *Theor. Appl. Climatol.*, **119**, 757–769, <https://doi.org/10.1007/s00704-014-1146-7>.
- Newton, R., and W. J. Randel, 2020: Observations of upper-tropospheric temperature inversions in the Indian monsoon and their links to convectively forced quasi-stationary Kelvin waves. *J. Atmos. Sci.*, **77**, 2835–2846, <https://doi.org/10.1175/JAS-D-20-0042.1>.
- Nishi, N., E. Nishimoto, H. Hayashi, M. Shiotani, H. Takashima, and T. Tsuda, 2010: Quasi-stationary temperature structure in the upper troposphere over the tropical Indian Ocean inferred from radio occultation data. *J. Geophys. Res.*, **115**, D14112, <https://doi.org/10.1029/2009JD012857>.
- Nishida, M., A. Shimizu, T. Tsuda, C. Rocken, and R. H. Ware, 2000: Seasonal and longitudinal variations in the tropical tropopause observed with the GPS occultation technique (GPS/MET). *J. Meteor. Soc. Japan*, **78**, 691–700, https://doi.org/10.2151/jmsj1965.78.6_691.
- Noersomadi, N., and T. Tsuda, 2016: Global distribution of vertical wavenumber spectra in the lower stratosphere observed using high-vertical-resolution temperature profiles from COSMIC GPS radio occultation. *Ann. Geophys.*, **34**, 203–213, <https://doi.org/10.5194/angeo-34-203-2016>.
- , and —, 2017: Comparison of three retrievals of COSMIC GPS radio occultation results in the tropical upper troposphere and lower stratosphere. *Earth Planets Space*, **69**, 125, <https://doi.org/10.1186/s40623-017-0710-7>.
- , —, and M. Fujiwara, 2019: Influence of ENSO and MJO on the zonal structure of tropical tropopause inversion layer using high-resolution temperature profiles retrieved from COSMIC GPS radio occultation. *Atmos. Chem. Phys.*, **19**, 6985–7000, <https://doi.org/10.5194/acp-19-6985-2019>.
- Ohring, G., Ed., 2007: Achieving satellite instrument calibration for climate change (ASCI³). NIST Doc., 144 pp., <https://www.nist.gov/system/files/documents/2017/03/15/asic3.pdf>.
- , B. Wielicki, R. Spencer, B. Emery, and R. Datla, 2005: Satellite instrument calibration for measuring global climate change: Report of a workshop. *Bull. Amer. Meteor. Soc.*, **86**, 1303–1314, <https://doi.org/10.1175/BAMS-86-9-1303>.
- Okazaki, I., and K. Heki, 2012: Atmospheric temperature changes by volcanic eruptions: GPS radio occultation observations in the 2010 Icelandic and 2011 Chilean cases. *J. Volcanol. Geotherm. Res.*, **245–246**, 123–127, <https://doi.org/10.1016/j.jvolgeores.2012.08.018>.
- Paulik, L. C., and T. Birner, 2012: Quantifying the deep convective temperature signal within the tropical tropopause layer (TTL). *Atmos. Chem. Phys.*, **12**, 183–195, <https://doi.org/10.5194/acp-12-183-2012>.
- Pilch Kedzierski, R., K. Matthes, and K. Bumke, 2016: The tropical tropopause inversion layer: Variability and modulation by equatorial waves. *Atmos. Chem. Phys.*, **16**, 11 617–11 633, <https://doi.org/10.5194/acp-16-11617-2016>.
- Pirscher, B., U. Foelsche, B. C. Lackner, and G. Kirchengast, 2007: Local time influence in single-satellite radio occultation climatologies from Sun-synchronous and non-Sun-synchronous satellites. *J. Geophys. Res.*, **112**, D11119, <https://doi.org/10.1029/2006JD007934>.
- , —, M. Borsche, G. Kirchengast, and Y.-H. Kuo, 2010: Analysis of migrating diurnal tides detected in FORMOSAT-3/COSMIC temperature data. *J. Geophys. Res.*, **115**, D14108, <https://doi.org/10.1029/2009JD013008>.
- Pišoft, P., P. Šácha, J. Miksovsky, P. Huszar, B. Scherllin-Pirscher, and U. Foelsche, 2018: Revisiting internal gravity waves analysis using GPS RO density profiles: Comparison with temperature profiles and application for wave field stability study. *Atmos. Meas. Tech.*, **11**, 515–527, <https://doi.org/10.5194/amt-11-515-2018>.
- Prata, A. T., and Coauthors, 2020: Anak Krakatau triggers volcanic freezer in the upper troposphere. *Sci. Rep.*, **10**, 3584, <https://doi.org/10.1038/s41598-020-60465-w>.
- Randel, W. J., and F. Wu, 2005: Kelvin wave variability near the equatorial tropopause observed in GPS radio occultation measurements. *J. Geophys. Res.*, **110**, D03102, <https://doi.org/10.1029/2004JD005006>.
- , and E. J. Jensen, 2013: Physical processes in the tropical tropopause layer and their roles in a changing climate. *Nat. Geosci.*, **6**, 169–176, <https://doi.org/10.1038/ngeo1733>.
- , and F. Wu, 2015: Variability of zonal mean tropical temperatures derived from a decade of GPS radio occultation data. *J. Atmos. Sci.*, **72**, 1261–1275, <https://doi.org/10.1175/JAS-D-14-0216.1>.
- , and M. Park, 2019: Diagnosing observed stratospheric water vapor relationships to the cold point tropical tropopause. *J. Geophys. Res. Atmos.*, **124**, 7018–7033, <https://doi.org/10.1029/2019JD030648>.
- , F. Wu, and W. R. Ríos, 2003: Thermal variability of the tropical tropopause region derived from GPS/MET observations. *J. Geophys. Res.*, **108**, 4024, <https://doi.org/10.1029/2002JD002595>.
- , —, S. J. Oltmans, K. Rosenlof, and G. E. Nedoluha, 2004: Interannual changes of stratospheric water vapor and correlations with tropical tropopause temperatures. *J. Atmos. Sci.*, **61**, 2133–2148, [https://doi.org/10.1175/1520-0469\(2004\)061<2133:ICOSWV>2.0.CO;2](https://doi.org/10.1175/1520-0469(2004)061<2133:ICOSWV>2.0.CO;2).
- , D. J. Seidel, and L. L. Pan, 2007: Observational characteristics of double tropopauses. *J. Geophys. Res.*, **112**, D07309, <https://doi.org/10.1029/2006JD007904>.
- , R. R. Garcia, N. Calvo, and D. Marsh, 2009: ENSO influence on zonal mean temperature and ozone in the tropical lower stratosphere. *J. Geophys. Res.*, **36**, L15822, <https://doi.org/10.1029/2009GL039343>.
- Rapp, M., A. Dörnbrack, and B. Kaifler, 2018: An intercomparison of stratospheric gravity wave potential energy densities from METOP GPS radio occultation measurements and ECMWF model data. *Atmos. Meas. Tech.*, **11**, 1031–1048, <https://doi.org/10.5194/amt-11-1031-2018>.
- Ratnam, M. V., G. Tetzlaff, and C. Jacobi, 2004: Global and seasonal variations of stratospheric gravity wave activity deduced from the CHAMP/GPS satellite. *J. Atmos. Sci.*, **61**, 1610–1620, [https://doi.org/10.1175/1520-0469\(2004\)061<1610:GASVOS>2.0.CO;2](https://doi.org/10.1175/1520-0469(2004)061<1610:GASVOS>2.0.CO;2).
- , T. Tsuda, T. Kozu, and S. Mori, 2006: Long-term behavior of the Kelvin waves revealed by CHAMP/GPS RO measurements and their effects on the tropopause structure. *Ann.*

- Geophys.*, **24**, 1355–1366, <https://doi.org/10.5194/angeo-24-1355-2006>.
- , S. R. Babu, S. S. Das, G. Basha, B. V. Krishnamurthy, and B. Venkateswararao, 2016: Effect of tropical cyclones on the stratosphere–troposphere exchange observed using satellite observations over the north Indian Ocean. *Atmos. Chem. Phys.*, **16**, 8581–8591, <https://doi.org/10.5194/acp-16-8581-2016>.
- Ravindra Babu, S., M. V. Ratnam, G. Basha, B. V. Krishnamurthy, and B. Venkateswararao, 2015: Effect of tropical cyclones on the tropical tropopause parameters observed using COSMIC GPS RO data. *Atmos. Chem. Phys.*, **15**, 10 239–10 249, <https://doi.org/10.5194/acp-15-10239-2015>.
- Richter, J. H., F. Sassi, and R. R. Garcia, 2010: Toward a physically based gravity wave source parameterization in a general circulation model. *J. Atmos. Sci.*, **67**, 136–156, <https://doi.org/10.1175/2009JAS3112.1>.
- Rieckh, T., B. Scherllin-Pirscher, F. Ladstädter, and U. Foelsche, 2014: Characteristics of tropopause parameters as observed with GPS radio occultation. *Atmos. Meas. Tech.*, **7**, 3947–3958, <https://doi.org/10.5194/amt-7-3947-2014>.
- , R. Anthes, W. Randel, S.-P. Ho, and U. Foelsche, 2018: Evaluating tropospheric humidity from GPS radio occultation, radiosonde, and AIRS from high-resolution time series. *Atmos. Meas. Tech.*, **11**, 3091–3109, <https://doi.org/10.5194/amt-11-3091-2018>.
- Ringer, M. A., and S. B. Healy, 2008: Monitoring twenty-first century climate using GPS radio occultation bending angles. *Geophys. Res. Lett.*, **35**, L05708, <https://doi.org/10.1029/2007GL032462>.
- Rivoire, L., T. Birner, and J. A. Knaff, 2016: Evolution of the upper-level thermal structure in tropical cyclones. *Geophys. Res. Lett.*, **43**, 10 530–10 537, <https://doi.org/10.1002/2016GL070622>.
- Rocken, C., and Coauthors, 1997: Analysis and validation of GPS/MET data in the neutral atmosphere. *J. Geophys. Res.*, **102**, 29 849–29 866, <https://doi.org/10.1029/97JD02400>.
- , Y.-H. Kuo, W. S. Schreiner, D. Hunt, S. Sokolovskiy, and C. McCormick, 2000: COSMIC system description. *Terr. Atmos. Ocean. Sci.*, **11**, 21–52, [https://doi.org/10.3319/TAO.2000.11.1.21\(COSMIC\)](https://doi.org/10.3319/TAO.2000.11.1.21(COSMIC)).
- Šácha, P., U. Foelsche, and P. Pišhoft, 2014: Analysis of internal gravity waves with GPS RO density profiles. *Atmos. Meas. Tech.*, **7**, 4123–4132, <https://doi.org/10.5194/amt-7-4123-2014>.
- Sakazaki, T., K. Sato, Y. Kawatani, and S. Watanabe, 2015: Three-dimensional structures of tropical nonmigrating tides in a high-vertical-resolution general circulation model. *J. Geophys. Res. Atmos.*, **120**, 1759–1775, <https://doi.org/10.1002/2014JD022464>.
- Salby, M. L., and R. R. Garcia, 1987: Transient response to localized episodic heating in the tropics. Part I: Excitation and short-time near-field behavior. *J. Atmos. Sci.*, **44**, 458–498, [https://doi.org/10.1175/1520-0469\(1987\)044<0458:TRTLEH>2.0.CO;2](https://doi.org/10.1175/1520-0469(1987)044<0458:TRTLEH>2.0.CO;2).
- Sato, K., and T. J. Dunkerton, 1997: Estimates of momentum flux associated with equatorial Kelvin and gravity waves. *J. Geophys. Res.*, **102**, 26 247–26 261, <https://doi.org/10.1029/96JD02514>.
- Scherllin-Pirscher, B., G. Kirchengast, A. K. Steiner, Y.-H. Kuo, and U. Foelsche, 2011a: Quantifying uncertainty in climatological fields from GPS radio occultation: An empirical-analytical error model. *Atmos. Meas. Tech.*, **4**, 2019–2034, <https://doi.org/10.5194/amt-4-2019-2011>.
- , A. K. Steiner, G. Kirchengast, Y.-H. Kuo, and U. Foelsche, 2011b: Empirical analysis and modeling of errors of atmospheric profiles from GPS radio occultation. *Atmos. Meas. Tech.*, **4**, 1875–1890, <https://doi.org/10.5194/amt-4-1875-2011>.
- , C. Deser, S.-P. Ho, C. Chou, W. Randel, and Y.-H. Kuo, 2012: The vertical and spatial structure of ENSO in the upper troposphere and lower stratosphere from GPS radio occultation measurements. *Geophys. Res. Lett.*, **39**, L20801, <https://doi.org/10.1029/2012GL053071>.
- , A. K. Steiner, and G. Kirchengast, 2014: Deriving dynamics from GPS radio occultation: Three-dimensional wind fields for monitoring the climate. *Geophys. Res. Lett.*, **41**, 7367–7374, <https://doi.org/10.1002/2014GL061524>.
- , W. J. Randel, and J. Kim, 2017a: Tropical temperature variability and Kelvin-wave activity in the UTLS from GPS RO measurements. *Atmos. Chem. Phys.*, **17**, 793–806, <https://doi.org/10.5194/acp-17-793-2017>.
- , A. K. Steiner, G. Kirchengast, M. Schwarz, and S. Leroy, 2017b: The power of vertical geolocation of atmospheric profiles from GNSS radio occultation. *J. Geophys. Res. Atmos.*, **122**, 1595–1616, <https://doi.org/10.1002/2016JD025902>.
- Schmidt, T., J. Wickert, G. Beyerle, and C. Reigber, 2004: Tropical tropopause parameters derived from GPS radio occultation measurements with CHAMP. *J. Geophys. Res.*, **109**, D13105, <https://doi.org/10.1029/2004JD004566>.
- , S. Heise, J. Wickert, G. Beyerle, and C. Reigber, 2005: GPS radio occultation with CHAMP and SAC-C: Global monitoring of thermal tropopause parameters. *Atmos. Chem. Phys.*, **5**, 1473–1488, <https://doi.org/10.5194/acp-5-1473-2005>.
- , G. Beyerle, S. Heise, J. Wickert, and M. Rothacher, 2006: A climatology of multiple tropopauses derived from GPS radio occultations with CHAMP and SAC-C. *Geophys. Res. Lett.*, **33**, L04808, <https://doi.org/10.1029/2005GL024600>.
- , A. de la Torre, and J. Wickert, 2008a: Global gravity wave activity in the tropopause region from CHAMP radio occultation data. *Geophys. Res. Lett.*, **35**, L16807, <https://doi.org/10.1029/2008GL034986>.
- , J. Wickert, G. Beyerle, and S. Heise, 2008b: Global tropopause height trends estimated from GPS radio occultation data. *Geophys. Res. Lett.*, **35**, L11806, <https://doi.org/10.1029/2008GL034012>.
- , J.-P. Cammas, H. G. J. Smit, S. Heise, J. Wickert, and A. Haser, 2010a: Observational characteristics of the tropopause inversion layer derived from CHAMP/GRACE radio occultations and MOZAIC aircraft data. *J. Geophys. Res.*, **115**, D24304, <https://doi.org/10.1029/2010JD014284>.
- , J. Wickert, and A. Haser, 2010b: Variability of the upper troposphere and lower stratosphere observed with GPS radio occultation bending angles and temperatures. *Adv. Space Res.*, **46**, 150–161, <https://doi.org/10.1016/j.asr.2010.01.021>.
- , P. Alexander, and A. de la Torre, 2016a: Stratospheric gravity wave momentum flux from radio occultation. *J. Geophys. Res. Atmos.*, **121**, 4443–4467, <https://doi.org/10.1002/2015JD024135>.
- , L. Schoon, H. Dobslaw, K. Matthes, M. Thomas, and J. Wickert, 2016b: UTLS temperature validation of MPI-ESM decadal hindcast experiments with GPS radio occultations. *Met. Z.*, **25**, 673–683, <https://doi.org/10.1127/metz/2015/0601>.
- Schreiner, W., C. Rocken, S. Sokolovskiy, S. Syndergaard, and D. Hunt, 2007: Estimates of the precision of GPS radio occultations from the COSMIC/FORMOSAT-3 mission. *Geophys. Res. Lett.*, **34**, L04808, <https://doi.org/10.1029/2006GL027557>.

- , S. Sokolovskiy, D. Hunt, C. Rocken, and Y.-H. Kuo, 2011: Analysis of GPS radio occultation data from the FORMOSAT-3/COSMIC and MetOp/GRAS missions at CDAAC. *Atmos. Meas. Tech.*, **4**, 2255–2272, <https://doi.org/10.5194/amt-4-2255-2011>.
- , and Coauthors, 2020: COSMIC-2 radio occultation constellation: First results. *Geophys. Res. Lett.*, **47**, e2019GL086841, <https://doi.org/10.1029/2019GL086841>.
- Schröder, T., S. Leroy, M. Stendel, and E. Kaas, 2003: Validating the microwave sounding unit stratospheric record using GPS occultation. *Geophys. Res. Lett.*, **30**, 1734, <https://doi.org/10.1029/2003GL017588>.
- Schwarz, J. C., G. Kirchengast, and M. Schwaerz, 2017: Integrating uncertainty propagation in GNSS radio occultation retrieval: From bending angle to dry-air atmospheric profiles. *Earth Space Sci.*, **4**, 200–228, <https://doi.org/10.1002/2016EA000234>.
- Shangguan, M., W. Wang, and S. Jin, 2019: Variability of temperature and ozone in the upper troposphere and lower stratosphere from multi-satellite observations and reanalysis data. *Atmos. Chem. Phys.*, **19**, 6659–6679, <https://doi.org/10.5194/acp-19-6659-2019>.
- Shi, C., W. Cai, and D. Guo, 2017: Composition and thermal structure of the upper troposphere and lower stratosphere in a penetrating mesoscale convective complex determined by satellite observations and model simulations. *Adv. Meteor.*, **2017**, 6404796, <https://doi.org/10.1155/2017/6404796>.
- Shimizu, A., and T. Tsuda, 1997: Characteristics of Kelvin waves and gravity waves observed with radiosondes over Indonesia. *J. Geophys. Res.*, **102**, 26 159–26 171, <https://doi.org/10.1029/96JD03146>.
- Sjoberg, J. P., R. A. Anthes, and T. Rieckh, 2021: The three-cornered hat method for estimating error variances of three or more atmospheric data sets. Part I: Overview and evaluation. *J. Atmos. Oceanic Technol.*, <https://doi.org/10.1175/JTECH-D-19-0217.1>, in press.
- Solomon, S., J. S. Daniel, R. R. Neely III, J.-P. Vernier, E. G. Dutton, and L. W. Thomason, 2011: The persistently variable “background” stratospheric aerosol layer and global climate change. *Science*, **333**, 866–870, <https://doi.org/10.1126/science.1206027>.
- Son, S.-W., N. F. Tandon, and L. M. Polvani, 2011: The fine-scale structure of the global tropopause derived from COSMIC GPS radio occultation measurements. *J. Geophys. Res.*, **116**, D20113, <https://doi.org/10.1029/2011JD016030>.
- , Y. Lim, C. Yoo, H. H. Hendon, and J. Kim, 2017: Stratospheric control of the Madden-Julian oscillation. *J. Climate*, **30**, 1909–1922, <https://doi.org/10.1175/JCLI-D-16-0620.1>.
- Staten, P. W., and T. Reichler, 2008: Use of radio occultation for long-term tropopause studies: Uncertainties, biases, and instabilities. *J. Geophys. Res.*, **113**, D00B05, <https://doi.org/10.1029/2008JD009886>.
- Steiner, A. K., and G. Kirchengast, 2000: Gravity wave spectra from GPS/MET occultation observations. *J. Atmos. Oceanic Technol.*, **17**, 495–503, [https://doi.org/10.1175/1520-0426\(2000\)017<0495:GWSFGM>2.0.CO;2](https://doi.org/10.1175/1520-0426(2000)017<0495:GWSFGM>2.0.CO;2).
- , and —, 2005: Error analysis of GNSS radio occultation data based on ensembles of profiles from end-to-end simulations. *J. Geophys. Res.*, **110**, D15307, <https://doi.org/10.1029/2004JD005251>.
- , —, U. Foelsche, L. Kornblueh, E. Manzini, and L. Bengtsson, 2001: GNSS occultation sounding for climate monitoring. *Phys. Chem. Earth*, **26A**, 113–124, [https://doi.org/10.1016/S1464-1895\(01\)00034-5](https://doi.org/10.1016/S1464-1895(01)00034-5).
- , —, M. Borsche, U. Foelsche, and T. Schoengassner, 2007: A multi-year comparison of lower stratospheric temperatures from CHAMP radio occultation data with MSU/AMSU records. *J. Geophys. Res.*, **112**, D22110, <https://doi.org/10.1029/2006JD008283>.
- , —, B. C. Lackner, B. Pirscher, M. Borsche, and U. Foelsche, 2009: Atmospheric temperature change detection with GPS radio occultation 1995 to 2008. *Geophys. Res. Lett.*, **36**, L18702, <https://doi.org/10.1029/2009GL039777>.
- , B. C. Lackner, F. Ladstädter, B. Scherllin-Pirscher, U. Foelsche, and G. Kirchengast, 2011: GPS radio occultation for climate monitoring and change detection. *Radio Sci.*, **46**, RS0D24, <https://doi.org/10.1029/2010RS004614>.
- , and Coauthors, 2013: Quantification of structural uncertainty in climate data records from GPS radio occultation. *Atmos. Chem. Phys.*, **13**, 1469–1484, <https://doi.org/10.5194/acp-13-1469-2013>.
- , B. C. Lackner, and M. A. Ringer, 2018: Tropical convection regimes in climate models: Evaluation with satellite observations. *Atmos. Chem. Phys.*, **18**, 4657–4672, <https://doi.org/10.5194/acp-18-4657-2018>.
- , and Coauthors, 2020a: Consistency and structural uncertainty of multi-mission GPS radio occultation records. *Atmos. Meas. Tech.*, **13**, 2547–2575, <https://doi.org/10.5194/amt-13-2547-2020>.
- , and Coauthors, 2020b: Observed temperature changes in the troposphere and stratosphere from 1979 to 2018. *J. Climate*, **33**, 8165–8194, <https://doi.org/10.1175/JCLI-D-19-0998.1>.
- Stendel, M., 2006: Monitoring climate variability and change by means of GNSS data. *Atmosphere and Climate: Studies by Occultation Methods*, U. Foelsche, G. Kirchengast, and A. K. Steiner, Eds., Springer, 275–285.
- Stocker, M., F. Ladstädter, H. Wilhelmson, and A. K. Steiner, 2019: Quantifying stratospheric temperature signals and climate imprints from post-2000 volcanic eruptions. *Geophys. Res. Lett.*, **46**, 12 486–12 494, <https://doi.org/10.1029/2019GL084396>.
- Sun, B., A. Reale, D. J. Seidel, and D. C. Hunt, 2010: Comparing radiosonde and COSMIC atmospheric profile data to quantify differences among radiosonde types and the effects of imperfect collocation on comparison statistics. *J. Geophys. Res.*, **115**, D23104, <https://doi.org/10.1029/2010JD014457>.
- Sun, Y., and Coauthors, 2018: The FengYun-3C radio occultation sounder GNOS: A review of the mission and its early results and science applications. *Atmos. Meas. Tech.*, **11**, 5797–5811, <https://doi.org/10.5194/amt-11-5797-2018>.
- Suzuki, J., M. Fujiwara, T. Nishizawa, R. Shirooka, K. Yoneyama, M. Katsumata, I. Matsui, and N. Sugimoto, 2013: The occurrence of cirrus clouds associated with eastward propagating equatorial $n = 0$ inertia-gravity and Kelvin waves in November 2011 during the CINDY2011/DYNAMO campaign. *J. Geophys. Res. Atmos.*, **118**, 12 941–12 947, <https://doi.org/10.1002/2013JD019960>.
- Syndergaard, S., 1999: Retrieval analysis and methodologies in atmospheric limb sounding using the GNSS radio occultation technique. Danish Meteorological Institute Sci. Rep 99-6, 76 pp., <https://www.dmi.dk/fileadmin/Rapporter/SR/sr99-6.pdf>.
- Tegtmeier, S., and Coauthors, 2020: Temperature and tropopause characteristics from reanalyses data in the tropical tropopause layer. *Atmos. Chem. Phys.*, **20**, 753–770, <https://doi.org/10.5194/acp-20-753-2020>.

- Tian, B., C. O. Ao, D. E. Waliser, E. J. Fetzer, A. J. Mannucci, and J. Teixeira, 2012: Intraseasonal temperature variability in the upper troposphere and lower stratosphere from the GPS radio occultation measurements. *J. Geophys. Res.*, **117**, D15110, <https://doi.org/10.1029/2012JD017715>.
- Tradowsky, J. S., C. P. Burrows, S. B. Healy, and J. R. Eyre, 2017: A new method to correct radiosonde temperature biases using radio occultation data. *J. Appl. Meteor. Climatol.*, **56**, 1643–1661, <https://doi.org/10.1175/JAMC-D-16-0136.1>.
- Tsai, H.-F., T. Tsuda, G. A. Hajj, J. Wickert, and Y. Aoyama, 2004: Equatorial Kelvin waves observed with GPS occultation measurements (CHAMP and SAC-C). *J. Meteor. Soc. Japan*, **82**, 397–406, <https://doi.org/10.2151/jmsj.2004.397>.
- Tsuda, T., Y. Murayama, H. Wiryosumarto, S. W. B. Harijono, and S. Kato, 1994: Radiosonde observations of equatorial atmosphere dynamics over Indonesia: 1. Equatorial waves and diurnal tides. *J. Geophys. Res.*, **99**, 10 491–10 505, <https://doi.org/10.1029/94JD00355>.
- , M. Nishida, C. Rocken, and R. H. Ware, 2000: A global morphology of gravity wave activity in the stratosphere revealed by the GPS occultation data (GPS/MET). *J. Geophys. Res.*, **105**, 7257–7273, <https://doi.org/10.1029/1999JD901005>.
- , M. V. Ratnam, P. T. May, M. J. Alexander, R. A. Vincent, and A. MacKinnon, 2004: Characteristics of gravity waves with short vertical wavelengths observed with radiosonde and GPS occultation during DAWEX (Darwin Area Wave Experiment). *J. Geophys. Res.*, **109**, D20S03, <https://doi.org/10.1029/2004JD004946>.
- , —, T. Kozu, and S. Mori, 2006: Characteristics of 10-day Kelvin wave observed with radiosondes and CHAMP/GPS occultation during the CPEA campaign (April–May, 2004). *J. Meteor. Soc. Japan*, **84A**, 277–293, <https://doi.org/10.2151/jmsj.84A.277>.
- , L. Xian, H. Hayashi, and N. Noersomadi, 2011: Analysis of vertical wave number spectrum of atmospheric gravity waves in the stratosphere using COSMIC GPS radio occultation data. *Atmos. Meas. Tech.*, **4**, 1627–1636, <https://doi.org/10.5194/amt-4-1627-2011>.
- Ueyama, R., E. P. Gerber, J. M. Wallace, and D. M. W. Frierson, 2013: The role of high-latitude waves in the intraseasonal to seasonal variability of tropical upwelling in the Brewer–Dobson circulation. *J. Atmos. Sci.*, **70**, 1631–1648, <https://doi.org/10.1175/JAS-D-12-0174.1>.
- Vedel, H., and M. Stendel, 2003: On the direct use of GNSS refractivity measurements for climate monitoring. *Proc. Fourth Oerstedt Int. Science Team Conf. (OIST-4)*, Danish Meteorological Institute, Copenhagen, Denmark, 275–278.
- Verkhoglyadova, O. P., S. S. Leroy, and C. O. Ao, 2014: Estimation of winds from GPS radio occultations. *J. Atmos. Oceanic Technol.*, **31**, 2451–2461, <https://doi.org/10.1175/JTECH-D-14-00061.1>.
- Vespe, F., R. Pacione, and E. Rosciano, 2017: A novel tool for the determination of tropopause heights by using GNSS radio occultation data. *Atmos. Climate Sci.*, **7**, 301–313, <https://doi.org/10.4236/acs.2017.73022>.
- Virts, K. S., and J. M. Wallace, 2014: Observations of temperature, wind, cirrus, and trace gases in the tropical tropopause transition layer during the MJO. *J. Atmos. Sci.*, **71**, 1143–1157, <https://doi.org/10.1175/JAS-D-13-0178.1>.
- von Engel, A., 2006: A first test of climate monitoring with radio occultation instruments: Comparing two processing centers. *Geophys. Res. Lett.*, **33**, L22705, <https://doi.org/10.1029/2006GL027767>.
- , S. Healy, C. Marquardt, Y. Andres, and F. Sancho, 2009: Validation of operational GRAS radio occultation data. *Geophys. Res. Lett.*, **36**, L17809, <https://doi.org/10.1029/2009GL039968>.
- Wallace, J. M., and V. E. Kousky, 1968: Observational evidence of Kelvin waves in the tropical stratosphere. *J. Atmos. Sci.*, **25**, 900–907, [https://doi.org/10.1175/1520-0469\(1968\)025<0900:OEOKWI>2.0.CO;2](https://doi.org/10.1175/1520-0469(1968)025<0900:OEOKWI>2.0.CO;2).
- , R. L. Panetta, and J. Estberg, 1993: Representation of the equatorial stratospheric quasi-biennial oscillation in EOF phase space. *J. Atmos. Sci.*, **50**, 1751–1762, [https://doi.org/10.1175/1520-0469\(1993\)050<1751:ROTESQ>2.0.CO;2](https://doi.org/10.1175/1520-0469(1993)050<1751:ROTESQ>2.0.CO;2).
- Wang, B.-R., X.-Y. Liu, and J.-K. Wang, 2013: Assessment of COSMIC radio occultation retrieval product using global radiosonde data. *Atmos. Meas. Tech.*, **6**, 1073–1083, <https://doi.org/10.5194/amt-6-1073-2013>.
- Wang, D.-Y., and Coauthors, 2004: Cross-validation of MIPAS/ENVISAT and GPS-RO/CHAMP temperature profiles. *J. Geophys. Res.*, **109**, D19311, <https://doi.org/10.1029/2004JD004963>.
- Wang, K.-Y., S.-C. Lin, and L.-C. Lee, 2009: Immediate impact of the Mt Chaiten eruption on atmosphere from FORMOSAT-3/COSMIC constellation. *Geophys. Res. Lett.*, **36**, L03808, <https://doi.org/10.1029/2008GL036802>.
- Wang, L., and M. J. Alexander, 2009: Gravity wave activity during stratospheric sudden warmings in the 2007–2008 Northern Hemisphere winter. *J. Geophys. Res.*, **114**, D18108, <https://doi.org/10.1029/2009JD011867>.
- , and —, 2010: Global estimates of gravity wave parameters from GPS radio occultation temperature data. *J. Geophys. Res.*, **115**, D21122, <https://doi.org/10.1029/2010JD013860>.
- Wang, W., K. Matthes, T. Schmidt, and L. Neef, 2013: Recent variability of the tropical tropopause inversion layer. *Geophys. Res. Lett.*, **40**, 6308–6313, <https://doi.org/10.1002/2013GL058350>.
- , —, and —, 2015: Quantifying contributions to the recent temperature variability in the tropical tropopause layer. *Atmos. Chem. Phys.*, **15**, 5815–5826, <https://doi.org/10.5194/acp-15-5815-2015>.
- Ware, R., and Coauthors, 1996: GPS sounding of the atmosphere from low Earth orbit: Preliminary results. *Bull. Amer. Meteor. Soc.*, **77**, 19–40, [https://doi.org/10.1175/1520-0477\(1996\)077<0019:GSOTAF>2.0.CO;2](https://doi.org/10.1175/1520-0477(1996)077<0019:GSOTAF>2.0.CO;2).
- Wheeler, M., and G. N. Kiladis, 1999: Convectively coupled equatorial waves: Analysis of clouds and temperature in the wavenumber–frequency domain. *J. Atmos. Sci.*, **56**, 374–399, [https://doi.org/10.1175/1520-0469\(1999\)056<0374:CCEWAO>2.0.CO;2](https://doi.org/10.1175/1520-0469(1999)056<0374:CCEWAO>2.0.CO;2).
- Wickert, J., R. Galas, G. Beyerle, R. König, and C. Reigber, 2001a: GPS ground station data for CHAMP radio occultation measurements. *Phys. Chem. Earth*, **26**, 503–511, [https://doi.org/10.1016/S1464-1895\(01\)00092-8](https://doi.org/10.1016/S1464-1895(01)00092-8).
- , and Coauthors, 2001b: Atmosphere sounding by GPS radio occultation: First results from CHAMP. *Geophys. Res. Lett.*, **28**, 3263–3266, <https://doi.org/10.1029/2001GL013117>.
- , G. Beyerle, T. Schmidt, C. Marquardt, R. König, L. Grunwaldt, and C. Reigber, 2003: GPS radio occultation with CHAMP. *First CHAMP Mission Results for Gravity, Magnetic and Atmospheric Studies*, C. Reigber, H. Lühr, and P. Schwintzer, Eds., Springer, 371–383.
- , T. Schmidt, G. Beyerle, R. König, C. Reigber, and N. Jakowski, 2004: The radio occultation experiment aboard CHAMP: Operational data analysis and validation of vertical atmospheric profiles. *J. Meteor. Soc. Japan*, **82**, 381–395, <https://doi.org/10.2151/jmsj.2004.381>.

- , G. Beyerle, R. König, S. Heise, L. Grunwaldt, G. Michalak, C. Reigber, and T. Schmidt, 2005: GPS radio occultation with CHAMP and GRACE: A first look at a new and promising satellite configuration for global atmospheric sounding. *Ann. Geophys.*, **23**, 653–658, <https://doi.org/10.5194/angeo-23-653-2005>.
- Wilhelmsen, H., F. Ladstädter, B. Scherllin-Pirscher, and A. K. Steiner, 2018: Atmospheric QBO and ENSO indices with high vertical resolution from GNSS radio occultation temperature measurements. *Atmos. Meas. Tech.*, **11**, 1333–1346, <https://doi.org/10.5194/amt-11-1333-2018>.
- , —, T. Schmidt, and A. K. Steiner, 2020: Double tropopauses and the tropical belt connected to ENSO. *Geophys. Res. Lett.*, **47**, e2020GL089027, <https://doi.org/10.1029/2020GL089027>.
- WMO, 1957: Meteorology—A three dimensional science: Second session of the commission for aerology. *WMO Bull.*, **4**, 134–138.
- Wright, C. J., M. B. Rivas, and J. C. Gille, 2011: Intercomparisons of HIRDLS, COSMIC and SABER for the detection of stratospheric gravity waves. *Atmos. Meas. Tech.*, **4**, 1581–1591, <https://doi.org/10.5194/amt-4-1581-2011>.
- Xian, T., and Y. Fu, 2015: Characteristics of tropopause-penetrating convection determined by TRMM and COSMIC GPS radio occultation measurements. *J. Geophys. Res. Atmos.*, **120**, 7006–7024, <https://doi.org/10.1002/2014JD022633>.
- Xie, F., D. L. Wu, C. O. Ao, and A. J. Mannucci, 2010: Atmospheric diurnal variations observed with GPS radio occultation soundings. *Atmos. Chem. Phys.*, **10**, 6889–6899, <https://doi.org/10.5194/acp-10-6889-2010>.
- Xu, X., D. Yu, and J. Luo, 2018: The spatial and temporal variability of global stratospheric gravity waves and their activity during sudden stratospheric warming revealed by COSMIC measurements. *Adv. Atmos. Sci.*, **35**, 1533–1546, <https://doi.org/10.1007/s00376-018-5053-1>.
- Yanai, M., and T. Maruyama, 1966: Stratospheric wave disturbances propagating over the equatorial Pacific. *J. Meteor. Soc. Japan*, **44**, 291–294, https://doi.org/10.2151/jmsj1965.44.5_291.
- Yuan, L. L., R. A. Anthes, R. H. Ware, C. Rocken, W. D. Bonner, M. G. Bevis, and S. Businger, 1993: Sensing climate change using the global positioning system. *J. Geophys. Res.*, **98**, 14 925–14 937, <https://doi.org/10.1029/93JD00948>.
- Yulaeva, E., and J. M. Wallace, 1994: The signature of ENSO in global temperature and precipitation fields derived from the microwave sounding unit. *J. Climate*, **7**, 1719–1736, [https://doi.org/10.1175/1520-0442\(1994\)007<1719:TSOEIF>2.0.CO;2](https://doi.org/10.1175/1520-0442(1994)007<1719:TSOEIF>2.0.CO;2).
- Yunck, T. P., C.-H. Liu, and R. Ware, 2000: A history of GPS sounding. *Terr. Atmos. Ocean. Sci.*, **11**, 1–20, [https://doi.org/10.3319/TAO.2000.11.1.1\(COSMIC\)](https://doi.org/10.3319/TAO.2000.11.1.1(COSMIC)).
- Zeng, Z., W. Randel, S. Sokolovskiy, C. Deser, Y.-H. Kuo, M. Hagan, J. Du, and W. Ward, 2008: Detection of migrating diurnal tide in the tropical upper troposphere and lower stratosphere using the Challenging Minisatellite Payload radio occultation data. *J. Geophys. Res.*, **113**, D03102, <https://doi.org/10.1029/2007JD008725>.
- , S.-P. Ho, S. Sokolovskiy, and Y.-H. Kuo, 2012: Structural evolution of the Madden–Julian Oscillation from COSMIC radio occultation data. *J. Geophys. Res.*, **117**, D22108, <https://doi.org/10.1029/2012JD017685>.
- , S. Sokolovskiy, W. S. Schreiner, and D. Hunt, 2019: Representation of vertical structures by radio occultation observations in the upper troposphere and lower stratosphere: Comparison to high-resolution radiosonde profiles. *J. Atmos. Oceanic Technol.*, **36**, 655–670, <https://doi.org/10.1175/JTECH-D-18-0105.1>.
- Zhang, C., 2005: Madden–Julian oscillation. *Rev. Geophys.*, **43**, RG2003, <https://doi.org/10.1029/2004RG000158>.